



HAL
open science

Genotoxic impact of aluminum-containing nanomaterials in human intestinal and hepatic cells

Pégah Jalili, Sylvie Huet, Agnès Burel, Benjamin-Christoph Krause, Caroline Fontana, Soizic Chevance, Fabienne Gauffre, Yves Guichard, Alfonso Lampen, Peter Laux, et al.

► To cite this version:

Pégah Jalili, Sylvie Huet, Agnès Burel, Benjamin-Christoph Krause, Caroline Fontana, et al.. Genotoxic impact of aluminum-containing nanomaterials in human intestinal and hepatic cells. *Toxicology in Vitro*, 2022, 78, pp.105257. 10.1016/j.tiv.2021.105257 . hal-04249268

HAL Id: hal-04249268

<https://univ-rennes.hal.science/hal-04249268v1>

Submitted on 19 Oct 2023

HAL is a multi-disciplinary open access archive for the deposit and dissemination of scientific research documents, whether they are published or not. The documents may come from teaching and research institutions in France or abroad, or from public or private research centers.

L'archive ouverte pluridisciplinaire **HAL**, est destinée au dépôt et à la diffusion de documents scientifiques de niveau recherche, publiés ou non, émanant des établissements d'enseignement et de recherche français ou étrangers, des laboratoires publics ou privés.



Distributed under a Creative Commons Attribution - NonCommercial 4.0 International License

Genotoxic impact of aluminum-containing nanomaterials in human intestinal and hepatic cells.

Pégah JALILI^a, Sylvie HUET^a, Agnès BUREL^b, Benjamin-Christoph KRAUSE^c, Caroline FONTANA^d, Soizic CHEVANCE^e, Fabienne GAUFFRE^e, Yves GUICHARD^d, Alfonso LAMPEN^f, Peter LAUX^c, Andreas LUCH^c, Kevin HOGEVEEN^{a,g} and Valérie FESSARD^{a,*}
Valerie.fessard@anses.fr

^aANSES, French Agency for Food, Environmental and Occupational Health & Safety, Fougères Laboratory, Toxicology of Contaminants Unit, 10B rue C. Bourgelat, 35306 Fougères, France

^bMRic Cell Imaging Platform, BIOSIT, University of Rennes 1, campus Santé de Villejean, 2 avenue du Pr Léon Bernard - CS 34317, 35043 Rennes, France

^cFederal Institute for Risk Assessment (BfR), Department of Chemical and Product Safety, Max-Dohrn-Straße 8-10, 10589 Berlin, Germany

^dINRS, 1, rue du Morvan - CS 60027 - 54519 Vandoeuvre les Nancy, France

^eUniversité de Rennes 1, CNRS, ISCR (Institut des Sciences Chimiques de Rennes)-UMR6226, F-35000 Rennes, France

^fFederal Institute for Risk Assessment (BfR), Max-Dohrn-Straße 8-10, 10589 Berlin, Germany

^gASPIC Cellular Imaging Platform, 10B rue C. Bourgelat, 35306 Fougères, France

*Corresponding author at: Anses Laboratoire de Fougères Unité de Toxicologie des contaminants 10 B rue Claude Bourgelat, 35306 Fougères cedex, FRANCE

Abstract

Exposure of consumers to aluminum-containing nanomaterials (Al NMs) is an area of concern for public health agencies. As the available data on the genotoxicity of Al₂O₃ and Al⁰ NMs are inconclusive or rare, the present study investigated their *in vitro* genotoxic potential in intestinal and liver cell models, and compared with the ionic form AlCl₃. Intestinal Caco-2 and hepatic HepaRG cells were exposed to Al⁰ and Al₂O₃ NMs (0.03 to 80 µg/cm²). Cytotoxicity, oxidative stress and apoptosis were measured using High Content Analysis.

Genotoxicity was investigated through γ H2AX labelling, the alkaline comet and micronucleus assays. Moreover, oxidative DNA damage and carcinogenic properties were assessed using the Fpg-modified comet assay and the cell transforming assay in Bhas 42 cells respectively. The three forms of Al did not induce chromosomal damage. However, although no production of oxidative stress was detected, Al₂O₃ NMs induced oxidative DNA damage in Caco-2 cells but not likely related to ion release in the cell media. Considerable DNA damage was observed with Al⁰ NMs in both cell lines in the comet assay, likely due to interference with these NMs. No genotoxic effects were observed with AlCl₃. None of the Al compounds induced cytotoxicity, apoptosis, γ H2AX or cell transformation.

Keywords: nanomaterials; aluminum; nanotoxicology; comet assay; micronucleus; cell transformation assay

1. Introduction

Within the last decade, aluminum (Al)-containing nanomaterials (NMs) have been widely used not only for industrial applications, but also in consumer products, due to their higher reactivity compared to the bulk form (Li et al., 2014; Shepard and Brenner, 2013; Som et al., 2011; Willhite et al., 2014). Forms of Al, both in the micro- and the nano-size, are present in food and consumer products (Saiyed and Yokel, 2005; Willhite et al., 2014) due to their use as firming, anticaking, neutralizing, emulsifying and texturizing agents, as well as for cooking tools (Moradi et al., 2019), waste water treatment (European Food Safety, 2008; Kumar et al., 2011) and in medical and hygiene products such as toothpaste (Narayan et al., 2010; Zhang et al., 2017a; Zhao and Castranova, 2011). Nevertheless, their potential toxicity has not been fully evaluated, leading to major concerns from consumers and public health agencies (Laux et al., 2018).

According to exposure estimates from the European Food Safety Authority (EFSA), consumers can absorb up to 2.3 mg Al /kg bw/week, more than twice the weekly tolerable intake (TWI) (1 mg/kg bw/week) (European Food Safety, 2008). In addition, a recent study has estimated total consumer exposure to Al containing compounds, including contributions from products used in food (additives, contact materials) and in cosmetics, and concluded that most of the classes exceeded the EFSA-derived TWI, and that adolescents were highly exposed (Tietz et al., 2019).

Few studies on the genotoxicity of nanoscale forms of Al following oral ingestion have been performed, and most of the published literature has focused on Al₂O₃ NMs only. DNA damage was reported in erythrocytes of rats after a single oral treatment with Al₂O₃ NMs, although at high doses ($\geq 1,000$ mg/kg) (Balasubramanyam et al., 2009a; Balasubramanyam et al., 2009b). Genotoxic effects were observed in bone marrow, but not in other organs, after a short-term treatment with lower doses of Al₂O₃ NMs (Jalili et al., 2020). *In vivo* effects of Al⁰ NMs following oral exposure are mostly lacking, although one study suggested cross-linking effects on DNA in the duodenum of rats (Jalili et al., 2020). Following oral exposure of rodents with ionic forms of Al, an increase in micronucleus (MN) frequency was reported in bone marrow after a single oral administration (Paz et al., 2017) and in liver after a 30 day oral treatment (Turkez et al., 2010). Nevertheless, the induction of MN formation in liver was shown to decrease with an antioxidant treatment (Turkez et al., 2013; Turkez et al., 2010). Consistent with these results, a slight oxidative DNA damage was observed in blood after a short-term oral exposure (Jalili et al., 2020).

The *in vitro* genotoxicity of Al₂O₃ NMs has been assessed in several mammalian cell lines including human peripheral lymphocytes (Rajiv et al., 2016), primary human fibroblasts (Tsaousi et al., 2010), hepatic HepG2 cells (Alarifi et al., 2015), and Chinese hamster ovary

(CHO) cells (Di Virgilio et al., 2010). While some studies have not observed genotoxic effects of Al₂O₃ NMs (Demir et al., 2013; Hashimoto and Imazato, 2015; McKenna et al., 2003; Rajiv et al., 2016), others have reported a positive response (Alarifi et al., 2015; Tsaousi et al., 2010) which may be associated with oxidative damage (Alarifi et al., 2015). In contrast, data on the *in vitro* genotoxicity of Al⁰ NMs are scarce with no effect reported in the induction of genotoxic markers on human hepatic HepaRG and HepG2 cells (Sieg et al., 2019). For the salt AlCl₃, DNA damage has been reported in human peripheral blood lymphocytes, with positive results in micronucleus and chromosomal aberration tests, as well as in the comet assay (Banasik et al., 2005; Lankoff et al., 2006; Lima et al., 2007; Paz et al., 2017). However, no response of the genotoxic markers, phospho-ATM, phospho-p53 and phosphorylated histone H2AX (γ H2AX), was induced in HepaRG and HepG2 cells (Sieg et al., 2019).

According to an European Chemicals Agency (ECHA) safety assessment (ECHA), the data available on the genotoxicity of Al₂O₃ NMs are inconclusive while few data on the genotoxicity of Al NMs has been published so far. In addition to the direct contact of Al NMs present in food with the intestinal epithelium, Al accumulation in liver has been shown after oral exposure with Al₂O₃ NMs (Balasubramanyam et al., 2009b; Park et al., 2015; Shrivastava et al., 2014). Concerning carcinogenicity, although aluminum is not listed as a carcinogen (European Food Safety, 2008), certain exposures occurring during aluminium production cause cancer to humans (1987). Nevertheless, conflicting evidence on Al carcinogenicity has been pointed out. Although no association between Al and breast cancer was recently outlined, additional data on Al toxicity are requested (Klotz et al., 2017; Tietz et al., 2019).

Although we recently investigated the *in vivo* genotoxicity of Al NMs (Jalili et al., 2020), the *in vivo* treatment duration was rather short (3 administrations over 2 days), and it

cannot be excluded that the level of NMs in the organs would be low. Therefore, the aim of the current study was to complete the data on the genotoxicity of Al⁰ and Al₂O₃ NMs by evaluating their genotoxic potential in two relevant human cell models of intestine and liver. Intestinal Caco2 and liver HepaRG cell lines were used as they can differentiate into enterocytes and hepatocyte-like cells, and have been well characterized. These models have been previously used for genotoxicity testing with a long standing experience in the Anses laboratory (Bazin et al., 2010; Le Hégarat et al., 2010; Le Hégarat et al., 2006; Le Hégarat et al., 2014). Several endpoints of genotoxicity were investigated using the alkaline and formamidopyrimidine-DNA glycosylase (Fpg)-modified comet assays which detects DNA breakage including oxidative lesions, DNA double strand breaks were detected through γ H2AX, and the MN assay which determines chromosome and genome damage. Furthermore, the capacity of aluminum-containing NMs to initiate or promote carcinogenesis was assessed by the Cell Transforming Assay (CTA) in Bhas-42 cells.

As these NMs can potentially dissolve in the dispersion solution or in media, the genotoxicity was compared to that of the metal salt AlCl₃. Moreover, the interference of NMs, including with Al-NMs (Monteiro-Riviere et al., 2010), has been demonstrated in numerous publications using a wide range of biological assays, and stresses the necessity to evaluate interference in order to assess the potential effect on the results (Azqueta and Dusinska, 2015; Bessa et al., 2017; Di Bucchianico et al., 2017; Ferraro et al., 2016). In this study, various sources of interference have been taken into account within the different assays.

2. Materials and methods

2.1 Nanomaterials, chemicals and reagents

Al⁰, Al₂O₃ and zinc oxide (ZnO) NMs with a similar primary particle size were supplied from IoLiTec (Heilbronn, Germany). AlCl₃ (hexahydrate) was purchased from

Sigma Aldrich (Saint Louis, USA). Dimethylsulfoxide (DMSO), insulin, cytochalasin B, Fpg, trypan-blue, 12-*O*-tetradecanoylphorbol-13-acetate (TPA), 3-methylcholanthrene (3-MCA) and menadione (MEN) were supplied from Sigma (St. Quentin-Fallavier, France). Methyl methanesulfonate (MMS) was purchased by Acros Organics (Fairlawn, NJ). Dinophysistoxin-2 (DTX-2) was from the National Research Council Canada (NRCC, Ottawa, Canada). Penicillin, streptomycin, Williams' E medium and Fetal Bovine Serum Fetalclone II (FBS) were supplied from Invitrogen Corporation (Illkirch, France). For Bhas 42 cell cultures, Eagle's minimum essential medium and Dulbecco's modified Eagle's medium/Ham's F12 was from Invitrogen Corporation (Illkirch, France). Fetal bovine serum (FBS) was obtained by Dutscher, (Brumath France). Hydrocortisone hemisuccinate, Hyclone™ Dulbecco's Modified Eagle's Medium (DMEM)/high glucose and FBS for Caco-2 cells were purchased from Upjohn Pharmacia (Guyancourt, France), GE Healthcare Life Science (Logan, UT, USA) and Capricorn scientific (Ebsdorfergrund, Germany), respectively. The primary and secondary antibodies (mouse monoclonal anti γ H2AX ser139 (ab26350), rabbit monoclonal anti active caspase-3 antibody (ab13847), goat anti-rabbit IgG H&L AlexaFluor 647 (ab150079) and goat anti-mouse IgG H&L AlexaFluor 647 (ab150115)) were provided from Abcam (Cambridge, UK). CellROX® Deep Red Reagent was obtained from Invitrogen (Paisley, UK). Formaldehyde and Giemsa were purchased by Fisher (Illkirch-Graffenstaden, France).

2.2 Dispersion and characterization of NMs

NM characteristics as provided by the supplier are presented in **Error! Reference source not found.** A full characterization of the two AI NMs used in the present study was published in (Krause et al., 2018). NM dispersion was performed according to the NANOGENOTOX protocol (Hartmann et al., 2015), as described in (Jalili et al., 2020).

The morphology and agglomeration of Al⁰ and Al₂O₃ NMs in the stock dispersion solution and in cell media were determined by transmission electron microscopy (TEM) (Figure S 1). For the characterization of NMs from stock solutions, TEM grids were prepared immediately after sonication and dilution (100 µg/mL) in the stock dispersion solution. For the characterization of NMs in cell culture media (DMEM +10% FBS and William's Medium +5% FBS), the samples were diluted with distilled water to 1.2 µg/mL prior to grid preparation. The TEM grids were prepared by deposition of a carbon-coated copper grid onto a drop of the stock solution for 20 s to allow adsorption of the NMs and were observed with an electron microscope (JEOL 1400 operated at 120 kV and coupled with a 2k-2k camera from Gatan (Orios 1000)).

The hydrodynamic diameter (Z-Ave) of Al⁰ and Al₂O₃ NMs were measured using a Malvern Zetasizer (Malvern Instruments, Malvern, UK) equipped with a 633-nm laser diode operating at an angle of 173°. To assess the stability of NM suspensions, following NM dispersion, samples were diluted to a final concentration of 100 µg/mL in the stock dispersion solution or in cell media and measurements were performed at 0 and 24 h. The samples were equilibrated at 25 °C for 120 s prior to measurement. Ten repeated measurements for each sample were performed in 3 independent experiments. The mean hydrodynamic diameter Z-Ave was determined using cumulant analysis. Viscosity values used for the cell culture media were 0.97 cP for DMEM with 10% FCS and 0.96 cP for Williams with 5% FCS. The viscosity of water (0.89 cP) was used for stock solutions since it contains only 0.05% BSA.

No degradation of the Al NMs was reported in a previous study using an *in vitro* digestion system (Sieg et al., 2017).

2.3 Cell culture and treatment

The human colorectal adenocarcinoma Caco-2 cell line was cultured (passages 25–38) until differentiation after 21 days as described in (Jalili et al., 2018) including for cell seeding in various plate formats depending on the assay performed. Similarly, HepaRG cells (passages 13-19) were cultured and seeded for the various assays as previously described (Aninat et al., 2006; Jalili et al., 2018).

Differentiated Caco-2 and HepaRG cells were treated for 24 h with Al⁰ and Al₂O₃ NMs at concentrations ranging from 0.03 to 80 µg/cm² and with AlCl₃ as ionic salt control at 90 and 128 µg.mL⁻¹ in DMEM + 10% FBS or William's medium + 5% FBS respectively. For some assays, ZnO NMs at concentrations from 1.5 to 6 µg/cm² were used as a positive NM control. Equivalence between volume concentration (µg/mL) and surface concentration (µg/cm²) are shown in Table S 1B. Al content corresponding to the concentrations of Al-containing NMs and AlCl₃ that were used are summarized in Table S **Error! Reference source not found.1B**

2.4 Kinetics of nanoparticle sedimentation

The colloidal characterization of the suspended nanomaterials in the conditions of cellular uptake assay was achieved using the volumetric sedimentation method (VCM) as reported in DeLoid et al (DeLoid et al., 2017). We first measured the volume of the potentially agglomerated NM in DMEM and Williams media, at a NM concentration of 250 µg.mL⁻¹, using a specific centrifugal tube and ruler device. From the measured pellet, the effective density (ρ_{eff}) is calculated using the following equation:

$$\rho_{eff} = \rho_m + \left[\left(\frac{M_{NP}}{V \times SF} \right) \left(1 - \frac{\rho_m}{\rho_{NP}} \right) \right]$$

Where ρ_m is the density of the medium in g.cm⁻³, ρ_{NP} is the density of NP (2.7 g.cm⁻³ for Al and 3.95 for Al₂O₃), M_{NP} the total mass of NM in 1 mL of dispended volume and V the

measured volume pellet. The stacking factor (SF) was set to 0.634, which generally is appropriate for random stacking. The loss of mass of NMs from ion release was estimated to be lower than 1% and was neglected in the density calculation. The viscosity of the cell culture media at 37°C was determined using a Nanoparticle Tracking Analysis device (Malvern Instrument) by measuring the apparent hydrodynamic radius of 400 nm standard particles in the media. Finally, the kinetics of sedimentation was calculated using the distorted grid (DG) model available from DeLoid et al (DeLoid et al., 2017). The size of the NMs was taken from Table 2 (Z-Ave). Other model parameters are $h=3.1\text{mm}$ (liquid column height), initial NM concentration : $0.250\text{ mg}\cdot\text{mL}^{-1}$, the dissolution and cell-NMs stickiness are neglected (parameters set to 0).

2.5 Ion release from NMs

Following the dispersion of Al^0 and Al_2O_3 NMs, suspensions were diluted in stock solution (ultra pure water + 0.05 % bovine serum albumin (BSA)) or cell culture media (DMEM +10% FBS and William's Medium +5% FBS) at concentrations of 25, 50 and 100 $\mu\text{g}/\text{mL}$. After 24 h, ion release from NMs was determined by ultracentrifugation at 16,000 g for 1 h at 4°C (Hettich Zentrifuge Mikro 220R). The supernatants were processed through acidic hydrolysis (69% HNO_3 , 180°C for 20 min in an MLS-ETHOS Microwave system) before detection of Al species with a quadrupole Inductively Coupled Plasma Mass Spectrometry (ICP-MS) (iCAP Q, Thermo Fisher Scientific GmbH, Dreieich, Germany) equipped with a PFA ST Nebulizer, a quartz cyclonic spray chamber and a 2.5 mm quartz injector (Thermo Fisher Scientific). The gas flows were set to 14 L/min, and 0.65 L/min for the cool gas (Ar) and the auxiliary gas (Ar) respectively. The flow rate of the sample was 0.39 mL/min. Results are given as percentage of the initial Al amount.

2.6 Uptake observations by TEM

Following a 24 h treatment, cells were fixed by glutaraldehyde (2.5%) and embedded in DMP30-epon before cutting ultra-thin sections (90 nm) for TEM observation as described in (Jalili et al., 2018).

2.7 Cellular imaging and High Content Analysis (HCA)

After 24 h treatment with Al NMs and AlCl₃, plates were processed for HCA with an ArrayScan VTI HCS Reader (Thermo Scientific, Waltham, USA) as described in (Jalili et al., 2018). Cell numbers were determined from DAPI staining, active caspase-3 was quantified in the total cell compartment and γ H2AX in cell nuclei.

Oxidative stress was measured using CellROX Deep Red Reagent (Fisher Scientific, Illkirch, France). Briefly, cells were pre-incubated for 1 h with 5 μ M CellROX in serum-free media and washed twice with phosphate buffered saline (PBS) before treatment with NMs and AlCl₃. After 24 h and twice washing with PBS, cells were incubated with 3 μ M Hoescht 33342 for 20 min at 37°C. Cells were then washed twice with PBS and were scanned and analyzed using the Compartmental Analysis module of the Bioapplication software. For each well, images from 7 fields (20 \times magnification) were analyzed for quantification of fluorescence at 647 nm. ZnO NMs (6 μ g/cm²) and menadione (25 μ M for HepaRG and 50 μ M for Caco-2 cells) were used as positive controls.

2.8 Comet assay

After a 5 h (Figure S 3) or 24 h treatment with Al NMs and AlCl₃, the comet assay was performed as described in (Jalili et al., 2018; Le Hégarat et al., 2012). The individual tail intensity of at least 50 cells per slide were analyzed using the Comet Assay IV software (Perceptive Instruments, Haverhill, UK). Cells were considered as hedgehogs when DNA

damage was high and no clear head of the comet was observed. At least three independent experiments were performed. MMS (30 $\mu\text{g}/\text{mL}$, for 5 and 24h treatments) was used as positive control.

The level of oxidized bases was determined with the modified comet assay using the bacterial DNA repair enzyme Fpg through the formation of single-strand breaks induced by the excision of oxidized purines (Collins et al., 1993; Dušinská and Collins, 1996). Some additional steps to the protocol described above were performed such as incubation with enzyme buffer (0.1 M KCl, 0.2 mM EDTA, 40 mM HEPES, 0.2 mg/mL BSA) after lysis. Two slides, one incubated with enzyme buffer (control slide) and the other with 2000 U/mL Fpg at 37°C for 30 min, were then processed as described previously.

2.9 Particle interaction with DNA during the comet assay

The interaction of NMs with DNA migration during the comet assay was evaluated as described previously (Bessa et al., 2017; Jalili et al., 2018). Briefly, dilutions of Al^0 or Al_2O_3 NMs in 0.5% low-melting point agarose (LMP) were prepared at final concentrations of 28 and 128 $\mu\text{g}/\text{mL}$ (corresponding to 9 and 40 $\mu\text{g}/\text{cm}^2$ conditions). After trypsinization and centrifugation (2 min, 136 g), untreated Caco-2 and HepaRG cells were resuspended in the LMP/NM mixture, loaded on pre-coated slides and processed in the alkaline comet assay as previously described, in the presence or absence of Fpg. A negative control consisting of untreated cells in LMP-agarose in the absence of NMs was performed in order to compare the results.

2.10 Cytokinesis-block micronucleus assay (CBMN)

After a 24h-treatment, the CBMN assay was performed as described in (Jalili et al., 2018) according to the guideline n°487 of the Organization for Economic Co-operation and

Development (OECD) (OCDE, 2010). After staining of the slides with acridine orange (100 $\mu\text{g}/\text{mL}$), at least 1000 binucleated cells per slide were scored. Three independent experiments were carried out and each concentration was tested in duplicate. The replication index (RI) was calculated using the formula recommended by OCDE guideline n°487. MMS was used as positive control (25 $\mu\text{g}/\text{mL}$ for Caco-2 cells and 30 $\mu\text{g}/\text{mL}$ for HepaRG cells).

2.11 Bhas 42 Cell Transformation Assay (CTA)

Originally established from the v-Ha-ras-transfected BALB/c 3T3 cells by Sasaki et al (Sasaki et al., 1988), Bhas 42 cells used in this study (passage 23) were obtained from Harlan Laboratories (Rossdorf, Germany). Both the CTA and concurrent cell growth assays were performed in their 6-well format and in accordance with a guidance document produced by the OECD (OECD, 2017), with some modifications. The protocol, including both an initiation and a promotion assay, was previously described by Fontana et al (Fontana et al., 2017).

In the initiation assay, 24 h after seeding (420 cells/cm²) (Day 1), the cells were treated with Al NMs and AlCl₃ for 72 h (Day 4). Then, the cells were cultivated in fresh medium until Day 21, with medium changes on Day 7, Day 10 and Day 14. MCA (1 $\mu\text{g}/\text{mL}$) was used as positive control.

In the promotion assay, the cells were seeded (1,500 cells/cm²) and cultured for 4 days without changing the media. On Day 4, 7, and 10, the culture medium was replaced with fresh media containing Al NMs or AlCl₃. The treatment continued until Day 14. The cells were then cultured in fresh medium in the absence of NMs until Day 21. TPA (0.05 $\mu\text{g}/\text{mL}$) was used as positive control.

In both assays, the cells were fixed with ethanol on Day 21 and stained with a 5 % Giemsa solution. The morphological criteria recommended by OECD were followed for the

evaluation of transformed foci. The mean of the number of transformed foci was calculated from six replicate wells.

Cell growth assays in both the initiation and promotion conditions were performed on Day 7 using three replicate wells for each condition. The cells were fixed in 4% formaldehyde and stained with 1 $\mu\text{g}/\text{mL}$ DAPI. The number of cell in wells was determined by automated microscopy with an Arrayscan VTi using the Target Activation module of the BioApplication software. The relative cell growth (%) was calculated as follows: (number of cells in treated cultures / number of cell in control cultures) x100.

2.12 Statistical analysis

The statistical significance of HCA and comet assay results was tested using one-way Analysis of variance (ANOVA) followed by Dunnett's post-hoc tests with GraphPad Prism 5.

For the micronucleus assay, the percentages of micronucleated cells in treated and solvent control cultures were compared using the one-way Pearson chi-square test.

For the CTA, data were statistically analysed by multiple comparison using the one-sided Dunnett's test ($p < 0.05$, upper-sided). The significance of the positive controls (MCA and TPA) was evaluated relative to the control ($p < 0.05$) by the one-sided Student's t-test.

3. Results

3.1 Nanomaterial characterization

Information concerning the physico-chemical characterization, including the morphology, primary size, surface specific area (SSA), purity and density of the Al^0 , Al_2O_3 and ZnO NMs used in this study are provided in Table 1. However, in contrast to the information provided by the suppliers, the particle morphology of Al_2O_3 NMs in the stock dispersion solution cannot be considered as being spherical, but rather have a rod-like shape

when observed by TEM (Figure S1). Although Al⁰ particles exhibit a spherical shape, numerous elongated protrusions are also observed (Figure S1). Therefore, values of “average particle size” (Table 1) should then be considered with caution. Due to the drying step for preparation of TEM grids, the crystallization of different components of the culture media did not allow a proper characterization of the morphology of Al NMs in cell culture media (data not shown).

Particle hydrodynamic diameter (Z-Ave) in the stock dispersion solution, as well as in cell media, were assessed by Dynamic Light Scattering (DLS). Measurements were achieved immediately after dispersion (0 h), as well as after 24 h. In both cases, the dispersions were vortexed right before measurement, to resuspend sedimented particles, and the DLS measurements were analyzed by the Cumulant method. The Z-Ave and polydispersity index (PdI), which represents the width of the distribution in terms of hydrodynamic diameter: $PdI = (\text{Standard deviation} / \text{mean})^2$ are given in Table 2. Measurements of the NM in the stock solution immediately following dispersion yielded Z-Ave = 254 ± 4 nm for Al⁰, 168 ± 3 nm for Al₂O₃ and 233 ± 11 nm for ZnO. Although the three types of particles were supposed to have a similar primary size, we evidence that Al₂O₃ NMs have a smaller Z-Ave than Al⁰ and ZnO NMs. PdI was quite low (< 0.25) for all NMs in stock dispersion both at t=0 and after 24h. After 24h, the values for both Al-containing NMs were almost unchanged, indicating that no significant change of morphology of agglomeration state occurs within this period of time. However, the size of the ZnO NM appears about 20% lower after 24h, compared to t=0. This is also verified in the culture media, and could be due to partial solubilization of the ZnO. In contrast, the Z-Ave of the Al(0) NM is unchanged after 24H in all media. Al₂O₃ NMs, exhibit a different behavior, with no significant change after 24h in stock solution, but a

slightly larger size in both cell media. This increase in size is not accompanied with an increase in PDI, which could be due to protein adsorption.

The sedimentation of particles during *in vitro* exposure is critical when considering interactions of cells with NMs. Indeed, in a typical experiment the NMs are dispensed onto adherent cells in well plates. Therefore the amount of particles in contact with cells depends on the rate of sedimentation. We applied the dosimetry method reported by DeLoid et al (DeLoid et al., 2017) to evaluate the sedimentation of Al⁰ and Al₂O₃ NMs in DMEM and William's media in the conditions of cell exposure. When dispersed in culture medium, NMs may form agglomerates with adsorbed proteins and entrapped fluid. The effective density (ρ_{eff}) of these agglomerates should first be measured to determine the colloidal behavior of such agglomerates. The effective densities determined for Al⁰ NMs are 1.18 and 1.19 in DMEM and William's media respectively. Densities of 1.24 and 1.17 were obtained for Al₂O₃ NMs in DMEM and William's cell culture media respectively. Applying the sedimentation model provided in DeLoid et al (DeLoid et al., 2017), we calculated the evolution of the concentration of NMs at the surface of cells with respect to time (Figure 1). The sedimentation of Al⁰ NMs was similar in both media, and after 24 h the concentration at the bottom of the well is approximately 650 $\mu\text{g}/\text{mL}$. The rate of sedimentation of Al₂O₃ NMs was relatively slower, and the difference was significantly more pronounced in William's medium, with a deposited concentration of 450 $\mu\text{g}/\text{mL}$ at the bottom of the well after 24 h.

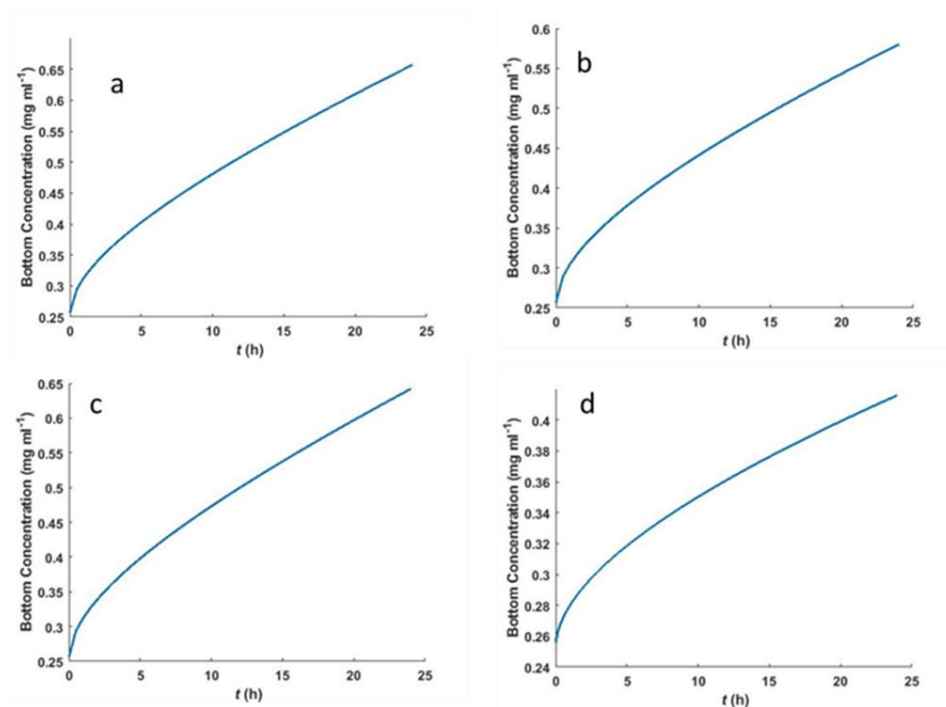


Figure 1: Time evolution over 24 h of the well-bottom concentration of (a) Al⁰ NMs in DMEM; (b) Al₂O₃ NMs in DMEM; (c) Al⁰ NMs in William's medium; (d) Al₂O₃ NMs in William's medium. Model parameters : bulk NM concentration 250 μ g/mL; T=37°C.

3.2 Ion release in stock solution and cell culture media

Ion release from Al NMs was investigated using ICP-MS (Table 3) and results are presented as percentages with respect to the initial concentration of aluminum. A decrease in the percentage of ion release from Al⁰ NMs was observed with increasing NMs concentrations in both the stock dispersion solution (1.30 % at 25 μ g/mL and 0.48 % at 100 μ g/mL) and in media (3.88 % to 0.95 % in DMEM, and 2.42 % to 0.68 % in William's for 25 and 100 μ g/mL respectively). Nevertheless, ion release from Al⁰ NMs was slightly higher in media when compared to the dispersion stock solution. A concentration-dependent decrease in ion release was also observed for ZnO NMs (Table 3). Ion release was also higher in media compared to dispersion stock solution.

In contrast to Al⁰ and ZnO NMs, for Al₂O₃ NMs, the percentage of ion release with respect to the initial concentration was very low, relatively stable and independent of the NM concentration, although ion release was slightly higher in cell media.

The level of ions from AlCl₃ solutions was stable and independent of the concentration in the stock solution, but decreased with increasing concentration in media. This decrease of ion concentration with higher concentrations is likely due to the precipitate formed by AlCl₃ in cell media.

3.3 Uptake of Al NMs in Caco-2 and HepaRG cells

The uptake and the intracellular distribution of Al⁰ and Al₂O₃ NMs following a 24 h treatment in Caco-2 and HepaRG cells were investigated by TEM (Figure 2 and 3). In both cell lines, the majority of Al⁰ NMs were found as dense agglomerates of various sizes in the cytoplasm embedded in electron lucent or dense vesicles which are likely endosomes and lysosomes (Figure 2 and 3, B and C, notched arrows). Moreover, in certain cases, some Al⁰ NMs were observed as isolated nanoparticle clusters in the cytoplasm proximal to the nucleus (Figure 2 and 3 C, full arrows). Observations of Al⁰ NMs in the nucleus were very rare, and this result requires further investigation as it may be due to artefacts. The distribution pattern observed for Al₂O₃ NMs was similar in both cell lines. While a perinuclear localization of Al₂O₃ NMs was also seen, this occurred less frequently than for Al⁰ NMs (Figure 2 and 3, D and E). Even at the lowest concentration, Al⁰ and Al₂O₃ NMs were internalized through vesicle formation, most likely endocytosis, and accumulated in the cytoplasm of Caco-2 and HepaRG cells (Figure S 2).

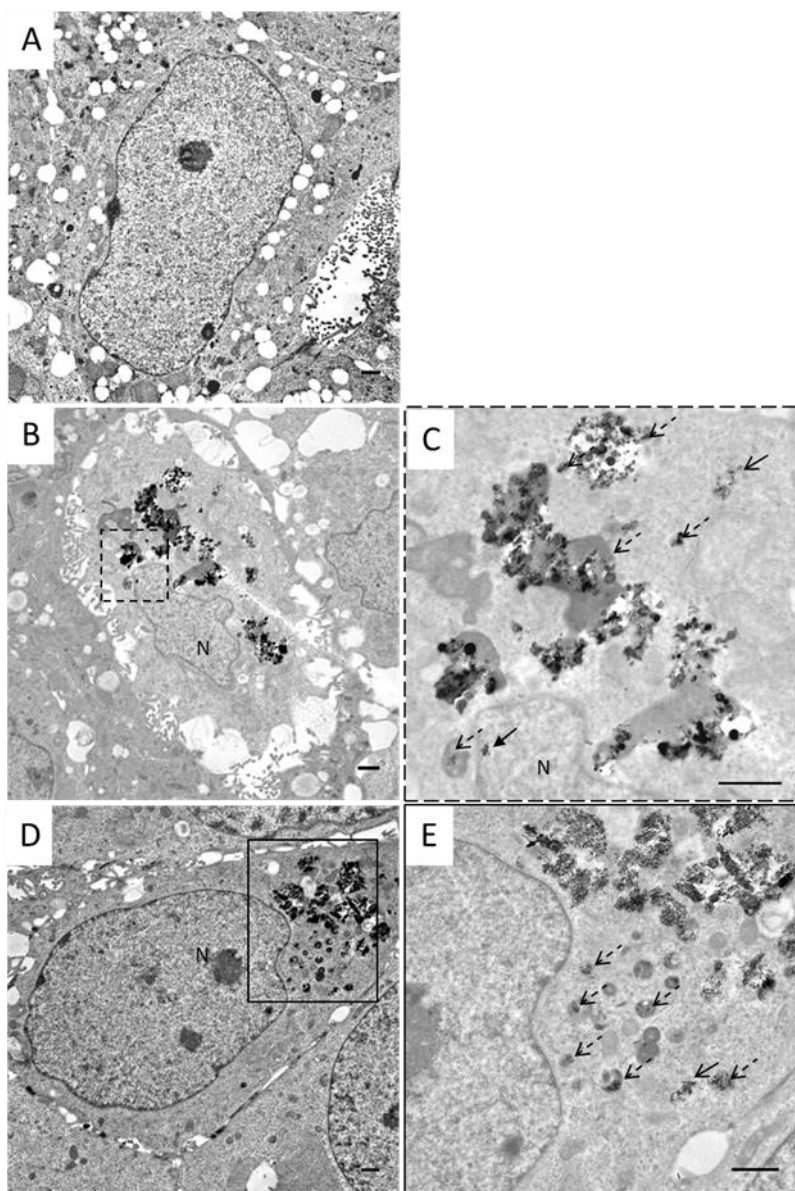


Figure 2: TEM images of differentiated Caco-2 cross-sections showing the uptake of Al^0 NMs (B, C) at $21 \mu g/cm^2$ and Al_2O_3 NMs (D,E) at $39 \mu g/cm^2$, after 24 h treatment compared to the negative control (A). Concentrations of $21 \mu g/cm^2$ Al^0 NMs and $39 \mu g/cm^2$ Al_2O_3 NMs were used to ensure equivalent Al content per well. C and E represent enlarged pictures from B and D respectively. C: Al^0 NMs were rarely seen in proximity to the nucleus (full arrow). C, E: NMs are present either in small clusters in the cytoplasm or near the nucleus (open arrow) either as large agglomerates integrated into lucent or dense vesicles (notched arrows).

These images are representative of the whole dataset. Scale bar 1 μm , C: Cytoplasm, N: nucleus.

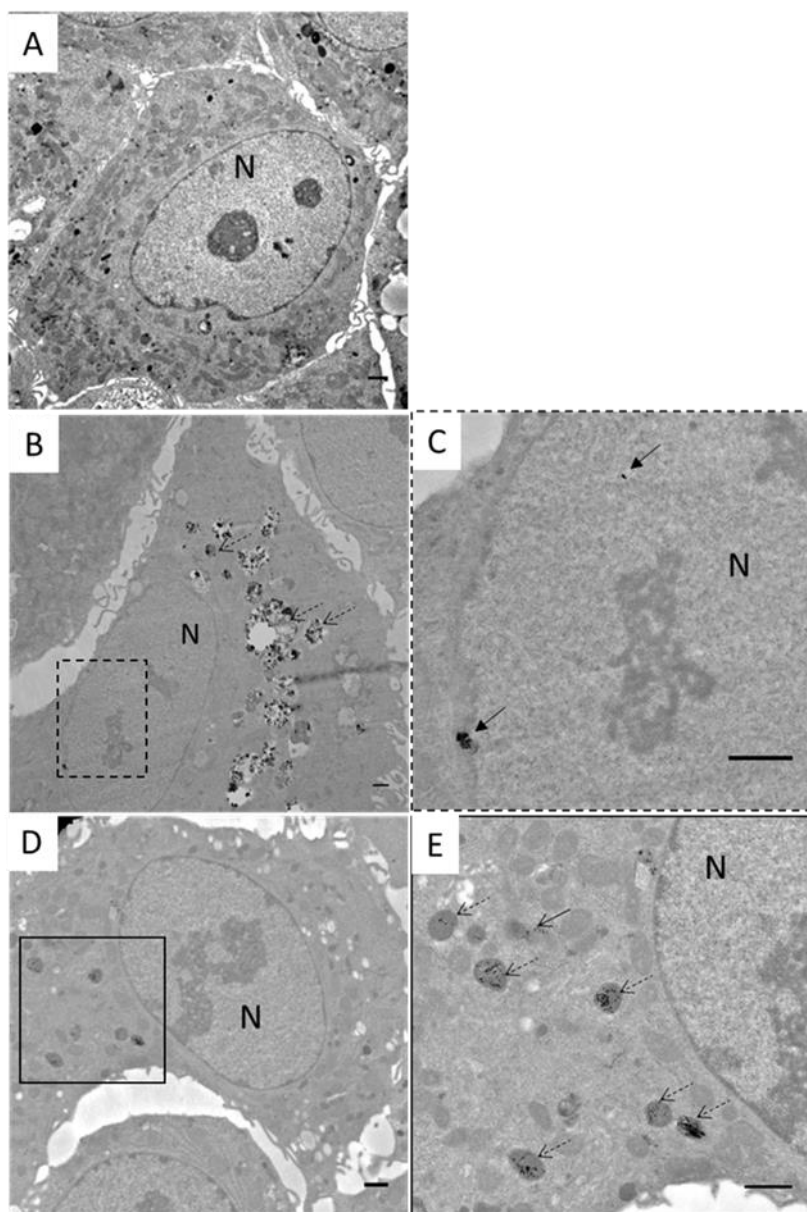


Figure 3: TEM images of differentiated HepaRG cross sections showing the uptake of Al^0 (B, C) at $21 \mu\text{g}/\text{cm}^2$ and Al_2O_3 (D,E) at $39 \mu\text{g}/\text{cm}^2$, after 24 h cell treatment compared to the negative control (A). Concentrations of $21 \mu\text{g}/\text{cm}^2$ Al^0 NMs and $39 \mu\text{g}/\text{cm}^2$ Al_2O_3 NMs were used to ensure equivalent Al content per well. C and E represent enlarged pictures from B and D respectively. C: Al^0 NMs were rarely seen near the nucleus (full arrow). E: NMs are included in vesicles containing large agglomerates (notched arrows) or as dense vesicles

containing small clusters in the cytoplasm (open arrow) or as isolated clusters. These images are representative of the whole dataset. Scale bar 1 μ m, C: Cytoplasm, N: nucleus.

3.4 Cytotoxicity

Viability and apoptosis in Caco-2 and HepaRG cells following a 24 h treatment with Al NMs were investigated by cell counts (Figure 4 A) and active caspase-3 labeling (Figure 4 B) respectively using automated image analysis. No significant change in cell numbers and active caspase-3 levels were observed in either Caco-2 or HepaRG cells treated with Al⁰ and Al₂O₃ NMs up to 80 μ g/cm². In addition, no significant cytotoxic effects were observed in cells treated with the ionic salt control AlCl₃ up to 128 μ g/mL Al content (1.16 mg/mL AlCl₃).

Similarly, no significant change in cell numbers were observed in Caco-2 cells treated with ZnO at the concentrations tested. However, a significant decrease in cell numbers as well as an increase in active caspase-3 levels was observed for the highest dose (6 μ g/cm²) of ZnO NMs in HepaRG cells.

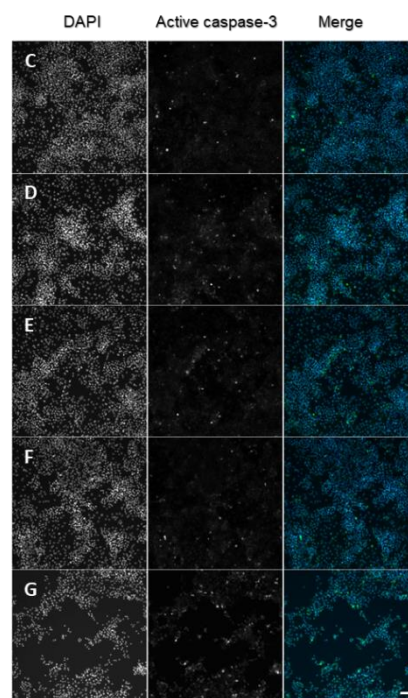
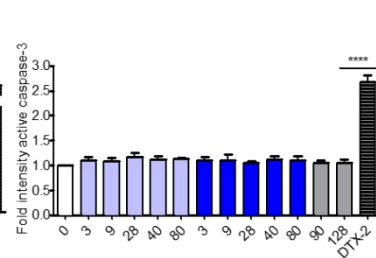
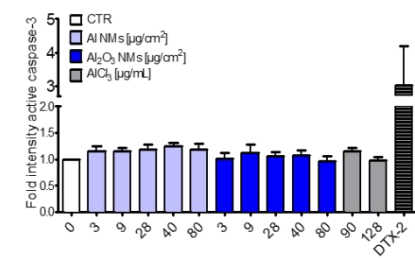
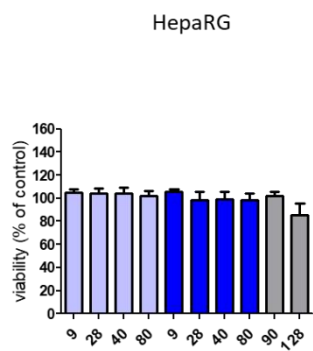
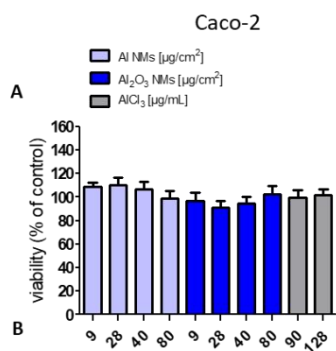


Figure 4: Effects of Al-containing NMs on cell numbers and active caspase-3 levels in differentiated Caco-2 and HepaRG cells. Cells were treated for 24 h with Al⁰ NMs, Al₂O₃ NMs and AlCl₃ as ionic salt control. ZnO and DTX-2 (20 nM for Caco-2 cells, 15 nM for HepaRG) were used as positive controls. Cell numbers (A) and active-caspase-3 (B) from automated image analysis are presented as fold changes relative to untreated cells. Representative images of active caspase-3 (green) in the cytoplasm of HepaRG cells are shown. C) negative control, D) Al⁰ NMs 80 µg/cm², E) Al₂O₃ NMs 80 µg/cm², F) AlCl₃ 128 µg/mL, G) ZnO NMs 6 µg/cm². Data are presented as the means ± SEM of 3 (Caco-2) or 4 (HepaRG) independent experiments. ****p < 0.0001. The images are representative of the whole dataset. White bar = 100 µm

3.5 Oxidative stress

Quantification of intracellular reactive oxygen species (ROS) was used to evaluate oxidative stress in Caco-2 and HepaRG cells following a 24 h treatment (Figure 5).

Intracellular ROS levels were not significantly changed following treatment up to 80 µg/cm² with Al⁰ and Al₂O₃ NMs or the ionic salt control AlCl₃. However, treatment with ZnO NMs significantly increased levels of ROS at the highest concentration (6 µg/cm²) in HepaRG cells.

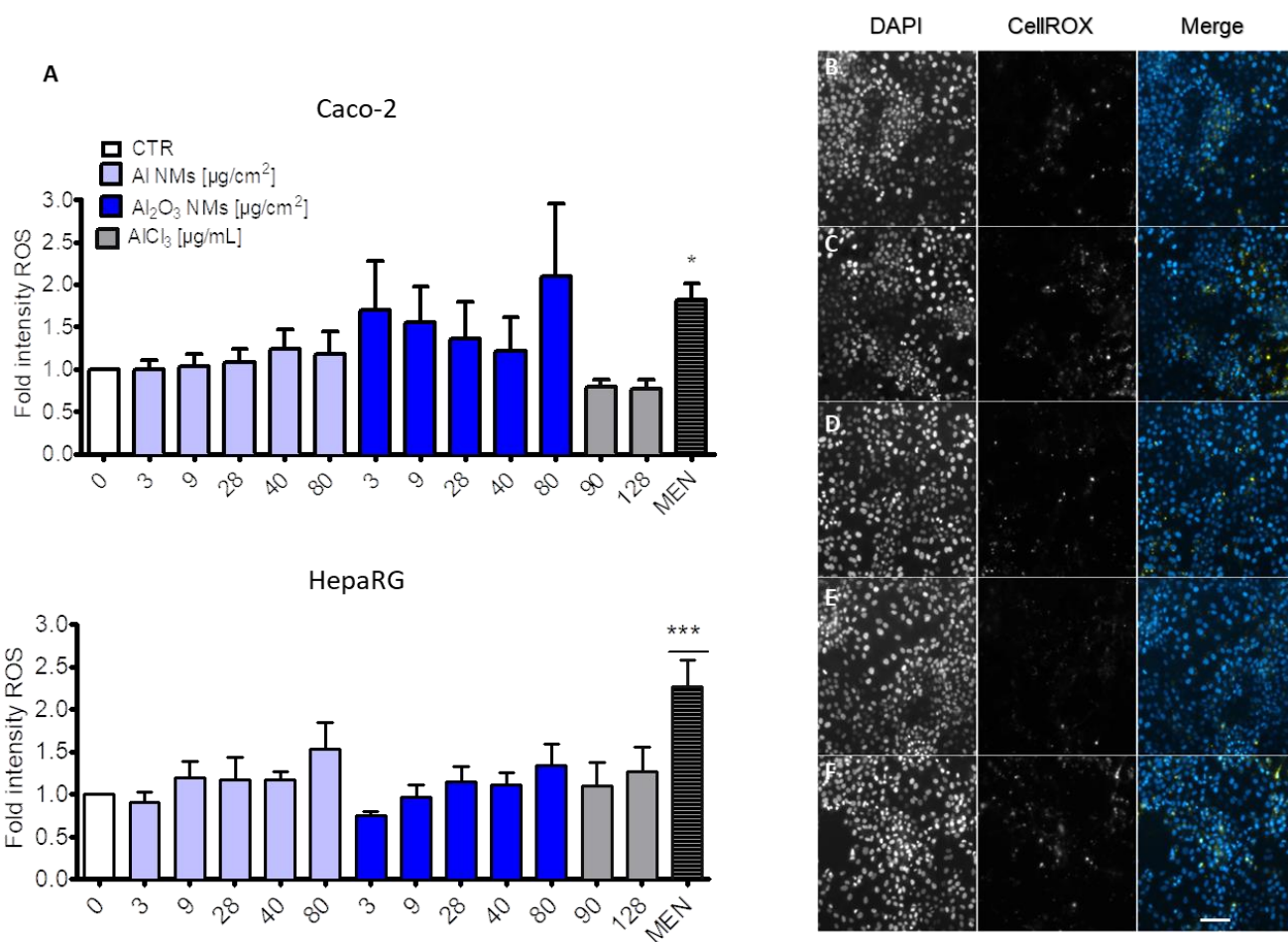


Figure 5: Effects of Al-containing NMs on ROS levels in differentiated Caco-2 and HepaRG cells. A) Cells were treated for 24 h with Al⁰ NMs, Al₂O₃ NMs and AlCl₃ as ionic salt control. ZnO and Menadione (MEN) (25 μM for HepaRG, 50 μM for Caco-2 cells) were used as positive controls. Representative images of ROS detection (yellow) in the cytoplasm of HepaRG cells are shown. B) negative control, C) Al⁰ NMs 80 μg/cm², D) Al₂O₃ NMs 80 μg/cm², E) AlCl₃ (128 μg/mL), F) ZnO NMs 6 μg/cm². Data are presented as the means ± SEM of 5 (Caco-2) or 6 (HepaRG) independent experiments. *p< 0.05, ***p<0.001. The images are representative of the whole dataset. White bar = 100 μm.

3.6 Genotoxicity

3.6.1 γH2AX

Quantification of γ H2AX labeling was used to evaluate the induction of DNA double strand breaks in Caco-2 and HepaRG cells following a 24 h treatment with Al NMs. Compared to untreated cells, the γ H2AX levels were not affected in the nuclei of Caco-2 cells treated for 24 h with Al⁰ and Al₂O₃ NMs up to 80 μ g/cm², with ZnO NMs, or with the ionic salt control AlCl₃ up to 128 μ g/mL (Figure 6). However in HepaRG cells, Al⁰ NMs induced a slight but statistically significant increase in γ H2AX levels at the highest concentration (80 μ g/cm²) tested. ZnO NMs induced significant increases at 3 and 6 μ g/cm².

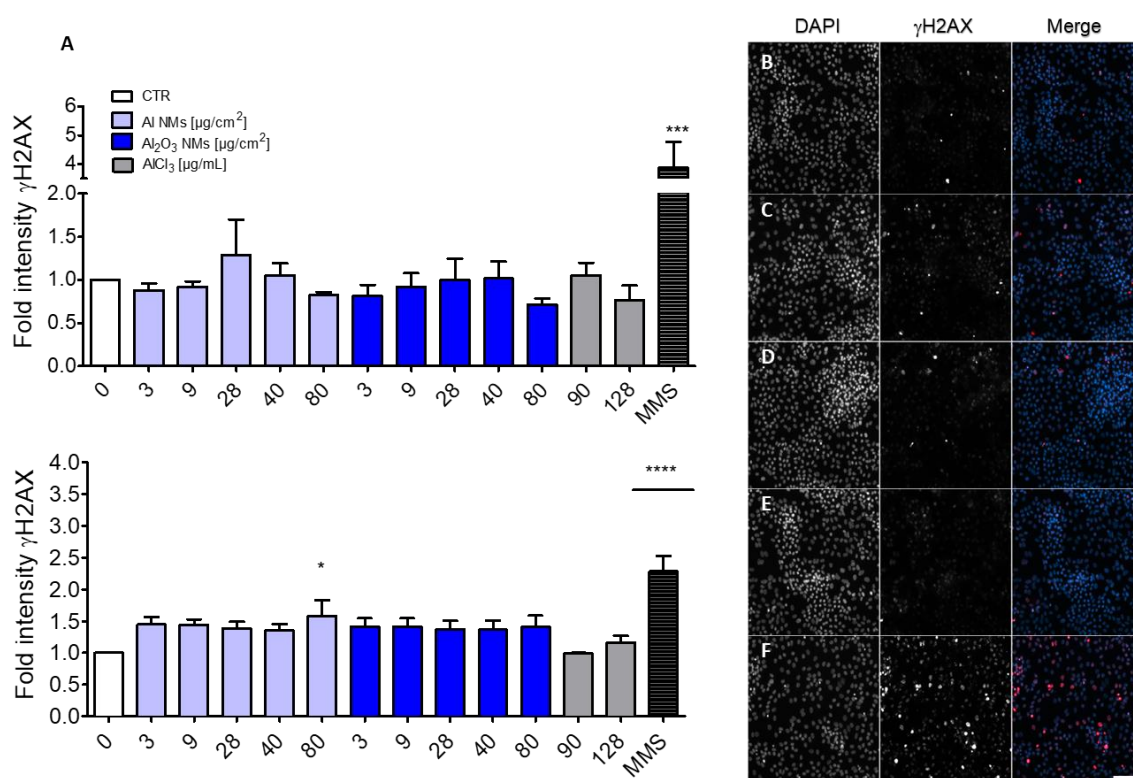


Figure 6: Effects of Al-containing NMs on γ H2AX level in Caco-2 and HepaRG Cells. A) Cells were treated for 24 h with Al⁰ NMs, Al₂O₃ NMs and AlCl₃ as ionic salt control, or positive controls (MMS at 60 or 30 μ g/ml respectively, and ZnO NMs). Representative images of γ H2AX detection (red) in the nuclei of HepaRG cells: B) negative control, C) Al⁰ NMs 80 μ g/cm², D) Al₂O₃ NMs 80 μ g/cm², E) AlCl₃ 128 μ g/mL, F) ZnO NMs 6 μ g/cm². Data are presented as the mean \pm SEM of 3 independent experiments. *p< 0.05, ***p<0.001, ****p<0.0001. The images are representative of the whole dataset. White bar=100 μ m.

3.6.2 Comet assay

The potential for Al⁰ and Al₂O₃ NMs to induce DNA damage in Caco-2 and HepaRG cells was investigated with the alkaline comet assay after a 24 h treatment (Figure 7 A and B). A modified comet assay with the Fpg enzyme was also performed to detect oxidative DNA damage (Figure 7 C and D).

In Caco-2 cells, a significant increase in tail DNA was observed with Al⁰ NMs from 28 to 80 µg/cm² in the alkaline comet assay (Figure 7 A). In contrast, neither Al₂O₃ and ZnO NMs, or the ionic salt control AlCl₃ induced any significant increase in tail DNA. In the Fpg-modified comet assay, a significant increase in tail DNA was observed in cells treated with Al₂O₃ NMs at 3, 9 and 80 µg/cm² (Figure 7 C).

In HepaRG cells, tail DNA significantly increased in a dose-dependent manner in cells treated with Al⁰ NMs, including a very considerable effect starting at 28 µg/cm². In contrast, no effect was observed for cells treated with Al₂O₃ and ZnO NMs, or the ionic control AlCl₃ (Figure 7 B). Similarly, an increase in tail DNA in the Fpg-modified comet assay was observed for Al⁰ NMs at all concentrations tested with a very significant effect observed at concentrations above 9 µg/cm². No significant changes in tail DNA were detected in HepaRG cells treated with Al₂O₃ and ZnO NMs or AlCl₃ (Figure 7 D).

DNA damage in Caco-2 and HepaRG was also investigated by the alkaline comet assay after a 5 h treatment (Figure S 3). In Caco-2 cells, a concentration-dependent increase in tail DNA was observed in cells treated with Al⁰ NMs from 28 to 80 µg/cm². No effect was detected in cells treated with Al₂O₃ and ZnO NMs, or the ionic salt control AlCl₃. In HepaRG cells, a concentration-dependent increase was also observed with Al⁰ NMs from 9 to 80 µg/cm². In the Fpg-modified comet assay, an increase in tail DNA was detected in Caco-2 cells treated with Al⁰ NMs from 9 to 80 µg/cm² and with Al₂O₃ NMs at 3, 9 and 28 µg/cm². Interestingly, in HepaRG cells treated for 5 h with Al NMs, results from the Fpg-modified

comet assay showed that at every concentration tested, only hedgehogs were observed for all NMs (data not shown).

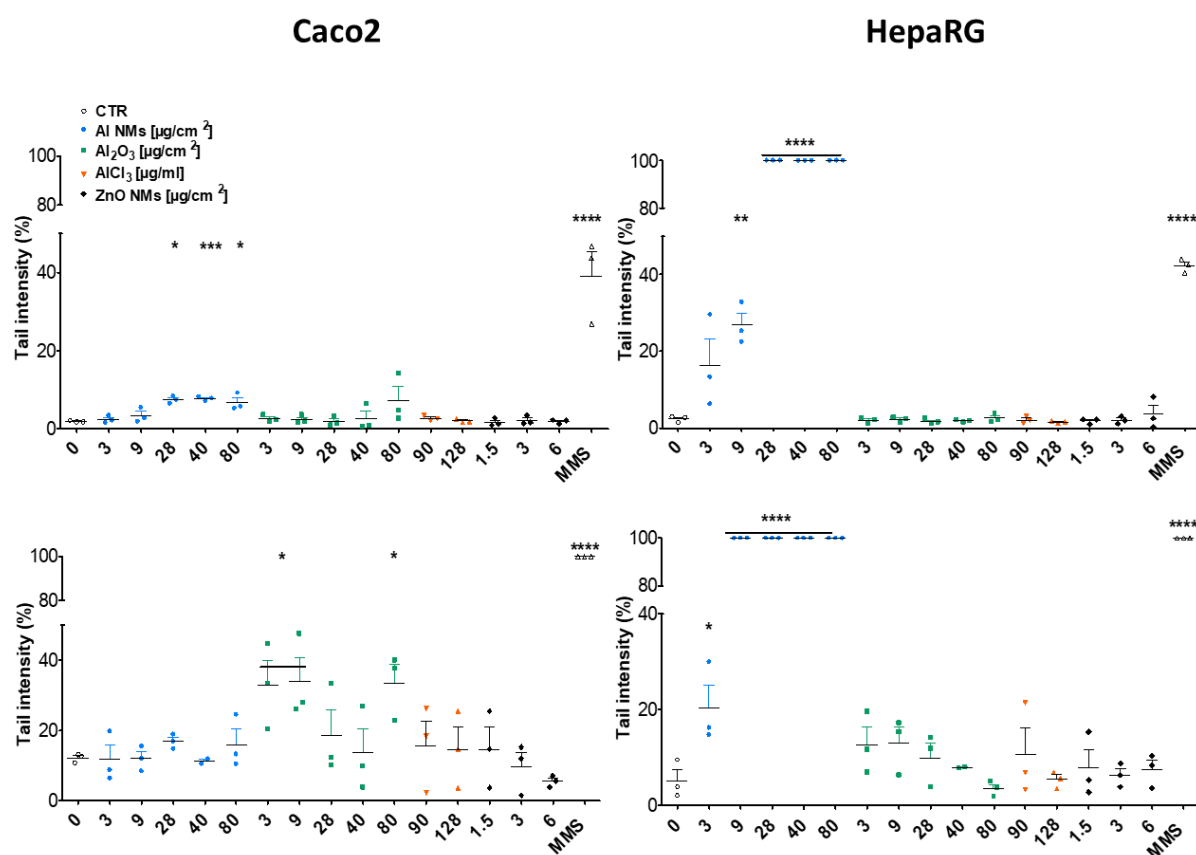


Figure 7: Detection of DNA damage in differentiated Caco-2 and HepaRG cells treated 24 h with Al-containing NMs with the alkaline and Fpg-modified comet assays. DNA damage (A, B) and oxidative DNA damage (C, D) were assessed in differentiated Caco-2 and HepaRG cells treated for 24 h with Al⁰, Al₂O₃ and ZnO NMs, and with the ionic salt control AlCl₃. MMS was used as a positive control (30 µg/mL). Values are presented as the mean percentage ± SEM of 3 independent experiments. *p < 0.05, **p < 0.01, ***p < 0.001, ****p < 0.0001

3.6.3 Interaction of NMs with DNA during the comet assay

The interference of NMs with the comet assay was assessed (Figure 8) according to the protocol described by Bessa et al (Bessa et al., 2017). Compared to the untreated control, a concentration-dependent increase in % tail DNA was observed when Al⁰ NMs are added at final concentrations of 9 and 40 µg/cm². A similar effect was also observed when Fpg was included in the assay. Compared to the negative control, no difference was detected for Al₂O₃ NMs in the absence of Fpg, while a slight increase was observed with Fpg.

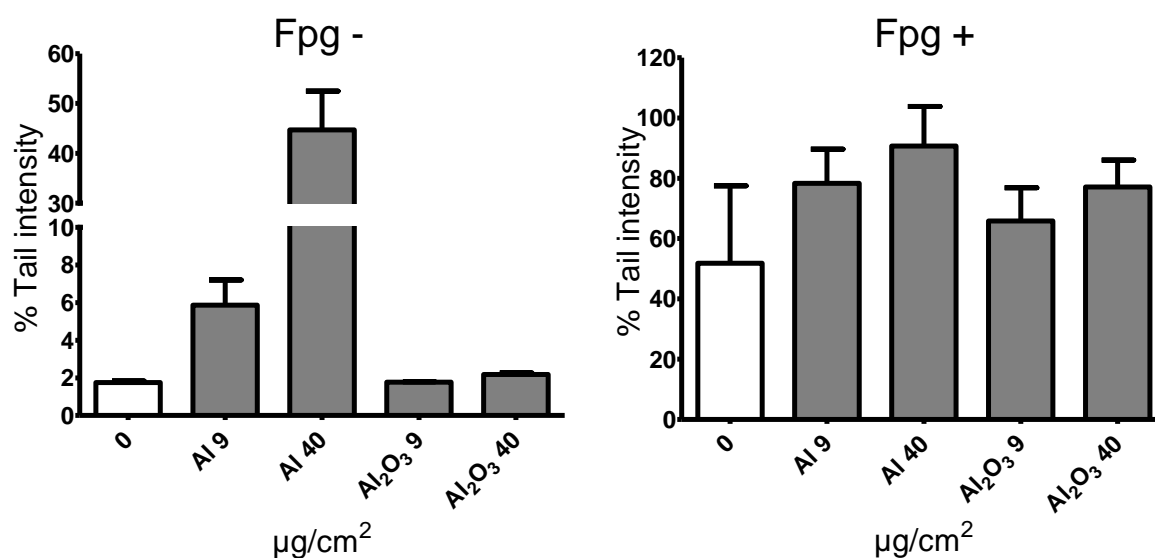


Figure 8: Interference of Al⁰ and Al₂O₃ NMs with the alkaline and Fpg-modified comet assays. The interference of Al⁰ and Al₂O₃ NMs with DNA migration was assessed with untreated HepaRG cells. NMs were added in LMP when cells are deposited on slides and compared with control (cells without addition of NMs). Values are presented as the mean percentage ± SEM of 2 independent experiments.

3.6.4 Micronucleus assay

In order to evaluate chromosome damage, the cytokinesis-block micronucleus assay was performed in Caco-2 and HepaRG cells treated for 24 h (Table 4) with Al NMs. No modification of cell viability (RI value) was observed in either Caco-2 or HepaRG cells

exposed to Al⁰, Al₂O₃, ZnO NMs and AlCl₃. Compared to the negative control, no significant increase in the percentage of binucleated micronucleated (BNMN) cells was detected in either cell line. Similarly, no increase in micronucleated mononucleated cells or in polyploid cells was observed (data not shown).

3.7 Bhas-42 Cell transforming (CTA) assay

Results of Bhas-42 CTA performed with Al⁰ and Al₂O₃ NMs and with AlCl₃ are shown in Table 5. In the initiation assay, both Al⁰ NMs and AlCl₃ induced a concentration-dependent decrease in cell proliferation on Day 7, inhibiting around 90% of cell proliferation at the highest concentration (3 µg/cm² for Al⁰ NMs and 28 µg/mL for AlCl₃). In contrast, Al₂O₃ NMs in the initiation assay and the three Al forms in the promotion assay induced no, or only a moderate, decrease in cell proliferation for all concentrations tested. No transforming activity was shown with the three Al forms, irrespective of the concentration tested in both the initiation and promotion assays. In contrast, the number of foci was found lower than those of controls at some concentrations of Al and Al₂O₃.

4. Discussion

Exposure of the general population to NMs present in consumer products, including food, has increased dramatically within the last decade, and a thorough evaluation of the potential adverse effects resulting from exposure to NMs following ingestion is necessary. Among the toxic effects of Al-containing NMs that have been shown in several studies, genetic damage is of particular concern (Alarifi et al., 2015; Balasubramanyam et al., 2009b; Di Virgilio et al., 2010; Tsaousi et al., 2010). Both intestine and liver are considered key organs for investigating genotoxic effect of nanomaterials found in food since they represent

the main organ of contact and the main organ of accumulation, respectively. Nevertheless, in our recent *in vivo* study, only a very limited genotoxic response was observed with Al⁰ NMs (Jalili et al., 2020) while no effect was detected on several genotoxicity markers *in vitro* (Sieg et al., 2019). Therefore, we chose to complete our study by investigating the *in vitro* genotoxicity of Al NMs in human intestinal Caco-2 and hepatic HepaRG cells using complementary tests.

Al₂O₃ NMs

Despite the uptake and presence of Al NMs in Caco-2 and HepaRG cells, no cytotoxicity or apoptotic response was observed following treatment with Al₂O₃ NMs. Our results are in agreement with data from various publications that have reported little or no cytotoxicity in various cell lines (Monteiro-Riviere et al., 2010; Radziun et al., 2011; Simon-Deckers et al., 2008; Tsaousi et al., 2010; Wagner et al., 2007), including in Caco-2 cells (Ivask et al., 2015; Sieg et al., 2018; Song et al., 2017), HepaRG (Sieg et al., 2019) and HepG2 cells (Alarifi et al., 2015; Sieg et al., 2019).

No induction of chromosomal damage was observed in the micronucleus assay in either Caco-2 or HepaRG cells exposed to Al₂O₃ NMs. Moreover, we did not observe a transforming activity in the CTA assay, supporting the absence of mutagenic potential for Al₂O₃ NMs. Our results are consistent with two recent studies that reported a negative response in the chromosomal aberration and the micronucleus assays in human lymphocytes treated with Al₂O₃ NMs with a smaller size (3 to 4 nm) than the one used in this study (20 nm), and for a longer incubation time (72 h) (Akbaba and Turkez, 2018; Rajiv et al., 2016). In contrast, other studies have reported an increase in micronucleus formation following a 24 h treatment with Al₂O₃ NMs in other cell lines, including CHO cells (Di Virgilio et al., 2010), human fibroblasts (Tsaousi et al., 2010) and RAW264 murine macrophages (Hashimoto and

Imazato, 2015). Interestingly, Al₂O₃ NMs were shown to inhibit the replication efficiency of high-fidelity DNA polymerase (Gao et al., 2019), although such inhibition did not affect the mutation rate at the single nucleotide level of replication products compared to controls (Gao et al., 2019). Further investigation demonstrated that Al₂O₃ NMs did not induce a clastogenic effect but rather chromosome loss and polyploidy, although these effects were observed only at one concentration (1 mg/mL) (Tsaousi et al., 2010). Considering the induction of polyploidy, mitosis or increase of micronucleated mononucleated cells, an aneugenic effect of Al NMs was not observed in our study (data not shown). The discrepancy may be explained by the fact that our treatments were performed in non-proliferating cells. The lack of chromosomal damage observed *in vitro* in our study following treatment with Al₂O₃ NMs is in agreement with results obtained from *in vivo* studies. In fact, with the same Al₂O₃ NMs used in this study, we did not observe an induction of micronuclei in either bone marrow or in the colon of rats after a short-term oral treatment (Jalili et al., 2020). Similarly, no induction of micronuclei in the bone marrow of mice was detected following intraperitoneal injections, irrespective of the size of the Al₂O₃ particles (Zhang et al., 2017b). In contrast, numerical chromosomal damage (aneuploidy and polyploidy) and abnormal metaphases were reported in the bone marrow of rats 48 hours after a single oral dose of Al₂O₃ NMs while no effect was observed with bulk Al₂O₃ (Balasubramanyam et al., 2009a; Balasubramanyam et al., 2009b). In addition, induction of micronuclei in erythrocytes was also observed. However, no toxicity on the bone marrow (determined by the frequency of polychromatic erythrocytes per total erythrocytes) was observed in the different studies (Balasubramanyam et al., 2009a; Balasubramanyam et al., 2009b; Jalili et al., 2020; Zhang et al., 2017b).

The absence of genotoxic activity of Al₂O₃ NMs in Caco-2 and HepaRG cells was further confirmed in the γ H2AX assay as well as the comet assay. We did not observe any increase in γ H2AX levels in either cell line, which is in agreement with results from a study

by Tsaousi et al (Tsaousi et al., 2010) in primary human fibroblasts. Additionally, Al₂O₃ NMs did not induce DNA damage in the alkaline comet assay in Caco-2 and HepaRG cells following a 24 h treatment. Although some studies have reported negative results in the comet assay in human lymphocytes and in human embryonic kidney cells (Demir et al., 2013; Rajiv et al., 2016), others have demonstrated time- and/or concentration-dependent genotoxic effects in Chinese hamster lung fibroblasts (Zhang et al., 2017b), in RAW264 murine macrophages (Hashimoto and Imazato, 2015) and in human liver HepG2 cells (Alarifi et al., 2015) treated with Al₂O₃ NMs. Nevertheless, the increase of DNA fragmentation in these latter studies was probably linked to cell death detected by Trypan blue exclusion (Zhang et al., 2017b) or by apoptotic markers (Alarifi et al., 2015; Hashimoto and Imazato, 2015). Moreover, interference of Al₂O₃ NMs was not checked in these publications which may also explain the discrepancy in the responses.

In vivo, after a short-term treatment using the same Al₂O₃ NMs, we only observed an increase in DNA damage in the comet assay in bone marrow, while no effect was observed in intestine, colon, kidney, spleen or blood (Jalili et al., 2020). Balasubramanyam et al (Balasubramanyam et al., 2009a) showed a time- and concentration-dependent increase in DNA damage in blood with the comet assay with both bulk and nano Al₂O₃ forms after a single gavage but the effect decreased at 48 h before disappearing at 72 h. DNA breakage associated with necrosis and apoptosis was observed in liver and kidney of rats after a repeated oral treatment for 75 days with 70 mg/kg bw Al₂O₃ NMs (Yousef et al., 2019). Therefore, it seems that both the *in vitro* and *in vivo* results with Al₂O₃ NMs support the conclusion that DNA breaks detected by the comet assay were mostly related to cell death rather than to a clear genotoxicity.

Nevertheless, we have shown that Al₂O₃ NMs induced oxidative DNA damage in Caco-2 cells following a 24 h treatment, despite no significant ROS induction. Furthermore, a

concentration-dependent trend towards oxidative damage was observed at 5 h. In previous studies, we already showed that no oxidative stress (reduced glutathione level and mitochondrial membrane potential) was detected in HepaRG and HepG2 cells as well as on differentiated Caco2 cells after 24h exposure to the same Al₂O₃ NMs (Sieg et al., 2018; Sieg et al., 2019). This could suggest the rapid formation of oxidative DNA damage which is further repaired, as previously demonstrated (Sadiq et al., 2015; Sliwinska et al., 2015). Evidence from *in vitro* experiments in a variety of different cell lines suggests that treatment with Al₂O₃ NMs can induce oxidative stress (Li et al., 2016; Rajiv et al., 2016; Shah et al., 2015; Zhang et al., 2017b) including in Caco2 cells (Song et al., 2017). Interestingly, Alarifi et al (Alarifi et al., 2015) reported positive results in the comet assay in HepG2 cells which was accompanied by oxidative damage and cell death. In the present study, no oxidative DNA damage or oxidative stress was observed in HepaRG cells. Differentiated HepaRG cells represent a model which is more similar to human hepatocytes when compared to HepG2 cells, and could therefore be less sensitive to oxidative damage resulting from Al₂O₃ NMs. In support of this, differences in the impact of ionic Al on oxidative stress was observed in HepG2 and HepaRG cells, with a clear reduction of GSH in HepG2 cells whereas no GSH reduction was detected in HepaRG cells (Sieg et al., 2019). Less information is available concerning the antioxidant capacity of Caco-2 cells, however HepG2 cells were more sensitive than Caco-2 cells to oxidative stress generated by hydrogen peroxide, tert-butylhydroperoxide and 2,2'-azobis (2-amidinopropane) (Martin et al., 1997). The higher antioxidant capacity of the cell lines used in our study could therefore explain the lack of oxidative stress observed following treatment with Al NMs.

Similarly, we did not detect oxidative DNA damage in liver, or in other organs of rats after oral exposure (Jalili et al., 2020). In contrast, an increase in oxidative stress was

observed in several tissues including liver after acute and repeated oral exposure of rats with Al₂O₃ NMs (Shrivastava et al., 2014).

Al⁰ NMs

Similar to the results obtained for Al₂O₃ NMs, no cytotoxicity or apoptotic response was observed following treatment with Al⁰ NMs, despite their presence in the cytoplasm of Caco-2 and HepaRG cells, as previously reported (Sieg et al., 2018; Sieg et al., 2019). In contrast to our results in differentiated Caco-2 and HepaRG cells, Al⁰ NMs were found to induce a decrease in viability in rat alveolar macrophages and in BRL3A rat liver cells following 24 h exposure at concentrations similar to those used in our study (Hussain et al., 2005; Wagner et al., 2007). This discrepancy could be explained by a difference in relative cell density for a similar concentration of Al⁰ NMs tested with a lower NM:cell ratio in differentiated Caco2 and HepaRG cells compared to the two other proliferating cell systems.

Despite only a slight increase in γ H2AX levels observed only in HepaRG cells and only at the highest concentration tested, a dose-dependent increase in tail DNA was observed in both Caco-2 and HepaRG cell lines treated with Al⁰ NMs using the alkaline comet assay after both 5 h and 24 h treatments. Nevertheless, this result required further investigation due to possible interference of NMs with the alkaline comet assay that has been widely documented in the literature (Azqueta and Dusinska, 2015; Bessa et al., 2017; Karlsson et al., 2015; Magdolenova et al., 2014). Indeed, NMs present in the cytoplasm of cells following uptake can interact with DNA following the lysis step of the comet assay, and could therefore induce additional breaks or inhibit DNA migration. In addition, a dissolution due to the conditions of the comet assay could result in reaction of Al ions with DNA, especially the phosphate backbone, as reported in some studies (Heli, 2014; Zhang et al., 2002). Such reactions may then induce DNA damage revealed during the comet assay as suggested by

Zhang et al (Zhang et al., 2009). Our results clearly demonstrate that, unlike Al₂O₃ NMs, Al⁰ NMs can induce DNA damage when in contact with DNA and interfere significantly with the comet assay. Consequently, the positive results in cells treated with Al⁰ NMs obtained in this study should therefore be treated with caution. *In vivo*, using the same Al⁰ NMs as the present study, no genotoxic response was observed in several key tissues, with the exception in rat duodenum where a cross-linking effect was suggested (Jalili et al., 2020).

The carcinogenic potential of Al NMs was investigated using the cell transformation assay with Bhas 42 cells. Neither Al⁰ nor Al₂O₃ NMs induced cell transformation, although a decrease in the number of transformed foci was observed. This decrease, observed at concentrations inducing a weak inhibition of cell proliferation at Day 7, is likely explained by a more pronounced inhibition of cell growth after 21 days of culture due to the three repeated treatments during the promotion assay. This phenomena was also observed with amorphous silica NMs (Fontana et al., 2017) as well as with other non-carcinogenic chemicals such as L-ascorbic acid and caffeine (Sakai et al., 2010).

Ion release from NMs in cell culture media, or in intracellular compartments can contribute to cytotoxic effects *in vitro*. The soluble fraction of Al⁰ and Al₂O₃ NMs measured by ICP-MS demonstrated a very low solubility of Al⁰ and Al₂O₃ NMs in both cell media. However, ion release may occur after cell uptake in specific compartments with low pH such as lysosomes (Sabella et al., 2014) as suggested for Al₂O₃ NMs (Hashimoto and Imazato, 2015). In such a scenario, secondary effects affecting mitochondria and resulting in the generation of ROS cannot be excluded. Consequently, effects could be induced by ionic Al released from the NMs rather than effects related to the particulate form (Willhite et al., 2014). As a strong oxygen acceptor, the Al ion tends to bind to citrate, phosphate, and catecholamine, generating oxygen radicals (Harris et al., 1996; Willhite et al., 2014). In addition, Al ions can also bind to negatively charged phospholipids, which are easily attacked

by reactive oxygen species such as $O_2^{\cdot-}$, H_2O_2 , and OH^{\cdot} (Verstraeten et al., 1997; Verstraeten and Oteiza, 2000) as well as DNA (Zhang et al., 2002). Although artificial simulation of the lysosomal compartment was not performed in our study, a previous study demonstrated that these same Al NMs did not dissolve significantly in an *in vitro* digestion system, even at low pH simulating stomach conditions (pH 2 for 2 hours with specific enzymes). In gastric media, metallic Al^0 nanoparticles released, slightly more ions (3 %), while Al_2O_3 nanoparticles were more inert in terms of solubility. Such behavior could be explained by the different surface of the two Al NMs as the formation of a passivating oxide layer on Al^0 NMs may influence its dissolution behavior (Krause et al., 2018). This very limited dissolution of Al NMs under acidic conditions therefore suggests that Al ions released from NMs do not contribute significantly to cytotoxic effects in our models.

$AlCl_3$

No genotoxic effects were observed in differentiated Caco-2 or HepaRG cells treated with $AlCl_3$ at concentrations up to 128 $\mu g/mL$ Al content corresponding to 1.16 mg/mL $AlCl_3$. At the concentrations of $AlCl_3$ tested, no effects were observed in the different assays following 5 or 24 h treatments. Indeed, negative results were obtained for promotion and initiation, as well as for genotoxic and oxidative stress responses. Our results are consistent with Villarini et al (Villarini et al., 2017) who observed no genotoxicity in response to Al ions in neuroblastoma cells with the comet assay, as well as no cytotoxicity or oxidative stress. We previously showed that $AlCl_3$ induced other markers of oxidative stress but without observation of DNA damage (phosphoATM, phospho-p53 and $\gamma H2AX$) in HepaRG and HepG2 cells (Sieg et al., 2019). However, other studies have reported genotoxicity of $AlCl_3$ in human lymphocytes (Lankoff et al., 2006; Paz et al., 2017). Interestingly, the authors of this study observed the highest level of micronuclei during the G1-phase of the cell cycle. The

differentiated HepaRG and Caco2 cells used in our study are not proliferating, and therefore could explain the discrepancy between the studies. *In vitro*, chromosomal damage observed in blood cells at AlCl₃ concentrations below 25 µg/mL, was associated with apoptosis (Banasik et al., 2005; Lankoff et al., 2006; Lima et al., 2007). Apoptosis was also observed in hepatic cells but mostly in HepG2 compared to HepaRG cells (Sieg et al., 2019). Moreover it was shown that Al ions can induce oxidative DNA damage irrespective of the cell cycle phase (Lankoff et al., 2006). Indeed, the role of Al ions in mediating genotoxic effects may be more complex, as it has been suggested that Al ions may inhibit several DNA repair proteins with zinc finger domains (Hanas and Gunn, 1996; Lankoff et al., 2006). Recently, a review on the genotoxicity of aluminum salts concluded that the absence of genotoxicity, even through oxidation (Jenkinson, 2021).

In our study, as the soluble fraction of AlCl₃ was always higher than that for Al⁰ and Al₂O₃ NMs, the effects observed for Al⁰ and Al₂O₃ NMs are not likely to be related to ion release in cell media. Although ECHA emphasized that the difference in the toxicological profile between soluble aluminum compounds and insoluble aluminum oxide may be explained by lower bioavailability of insoluble test compounds, it was recently shown that the content of Al in blood of rats treated orally was higher with Al₂O₃ NMs than with AlCl₃ (Krause et al., 2020). Moreover, the persistence of NMs in organs long after initial exposures has been described, and the accumulation of Al NMs in organs following repeated exposure could potentiate adverse effects in tissues in the long term. Further studies are clearly needed to investigate the fate of accumulated NMs in tissue, including possible effects due to ion release, as well as toxic effects related to particle accumulation.

5. Conclusions

In summary, despite the uptake and presence of Al NMs in the cytoplasm of differentiated Caco-2 and HepaRG cells, we have shown that Al₂O₃ NMs did not induce any toxic effects in a panel of assays, with the exception of an increase of oxidative DNA damage in Caco-2 cells. Similarly, the assays performed with Al⁰ NMs and AlCl₃ did not show a clear toxicity. However, it appears that Al⁰ NMs can induce DNA damage when in contact with DNA as observed in the comet assay when testing interference. As ion release from Al NMs was shown to be very limited in cell media, the effects are rather due to the particulate form or to ion release inside the cells. Further investigation is needed to clarify cytotoxic effects resulting from the direct impact of the presence of intracellular particles.

Author contributions

PJ and AB performed the electron microscopy study and analysis. BCK performed the experiments for dispersion and dissolution characterization. CF and YG performed and analysed the CTA. FG and SC performed the density and dispersion characterisation. PJ, SH and KH performed the genotoxicity experiments. PJ, BCK, FG, YG, KH and VF wrote the manuscript. AB, FG, AIL, PL, AnL, KH and VF wrote the proposal to obtain funding. All authors read and approved the final manuscript.

Declaration of Competing Interest

The authors declare that they have no competing interests.

Funding

This publication arises from the French-German bilateral project SolNanoTOX funded by the German Research Foundation (DFG, Project ID: DFG (FKZ LA 3411/1-1 respectively LA 1177/9-1) and the French National Research Agency (ANR, Project ID: ANR-13-IS10-0005).

Acknowledgements

The authors would like to thank Rachelle Lanceleur and Marie-Thérèse Lavault for technical assistance.

Declaration of interests

The authors declare that they have no known competing financial interests or personal relationships that could have appeared to influence the work reported in this paper.

The authors declare the following financial interests/personal relationships which may be considered as potential competing interests

References

1987. Aluminum production. IARC Monograph Suppl 7, 89-91.

Akbaba, G.B., Turkez, H., 2018. Investigation of the Genotoxicity of Aluminum Oxide, beta-Tricalcium Phosphate, and Zinc Oxide Nanoparticles In Vitro. *Int J Toxicol* 37, 216-222.

Alarifi, S., Ali, D., Alkahtani, S., 2015. Nanoalumina induces apoptosis by impairing antioxidant enzyme systems in human hepatocarcinoma cells. *International journal of nanomedicine* 10, 3751-3760.

Aninat, C., Piton, A., Glaise, D., Le Charpentier, T., Langouët, S., Morel, F., Guguen-Guillouzo, C., Guillouzo, A., 2006. Expression of cytochromes P450, conjugating enzymes and nuclear receptors in human hepatoma HepaRG cells. *Drug Metabolism and Disposition* 34, 75.

Azqueta, A., Dusinska, M., 2015. The use of the comet assay for the evaluation of the genotoxicity of nanomaterials. *Frontiers in genetics* 6, 239-239.

Balasubramanyam, A., Sailaja, N., Mahboob, M., Rahman, M.F., Hussain, S.M., Grover, P., 2009a. In vivo genotoxicity assessment of aluminium oxide nanomaterials in rat peripheral blood cells using the comet assay and micronucleus test. *Mutagenesis* 24, 245-251.

Balasubramanyam, A., Sailaja, N., Mahboob, M., Rahman, M.F., Misra, S., Hussain, S.M., Grover, P., 2009b. Evaluation of genotoxic effects of oral exposure to aluminum oxide nanomaterials in rat bone marrow. *Mutat Res* 676, 41-47.

Banasik, A., Lankoff, A., Piskulak, A., Adamowska, K., Lisowska, H., Wojcik, A., 2005. Aluminum-induced micronuclei and apoptosis in human peripheral-blood lymphocytes treated during different phases of the cell cycle. *Environ Toxicol* 20, 402-406.

Bazin, E., Mourot, A., Humpage, A.R., Fessard, V., 2010. Genotoxicity of a freshwater cyanotoxin, cylindrospermopsin, in two human cell lines: Caco-2 and HepaRG. *Environ Mol Mutagen* 51, 251-259.

Bessa, M.J., Costa, C., Reinoso, J., Pereira, C., Fraga, S., Fernández, J., Bañares, M.A., Teixeira, J.P., 2017. Moving into advanced nanomaterials. Toxicity of rutile TiO₂ nanoparticles immobilized in nanokaolin nanocomposites on HepG2 cell line. *Toxicol Appl Pharmacol* 316, 114-122.

Collins, A.R., Duthie, S.J., Dobson, V.L., 1993. Direct enzymic detection of endogenous oxidative base damage in human lymphocyte DNA. *Carcinogenesis* 14, 1733-1735.

DeLoid, G.M., Cohen, J.M., Pyrgiotakis, G., Demokritou, P., 2017. Preparation, characterization, and in vitro dosimetry of dispersed, engineered nanomaterials. *Nat Protoc* 12, 355-371.

Demir, E., Burgucu, D., Turna, F., Aksakal, S., Kaya, B., 2013. Determination of TiO₂, ZrO₂, and Al₂O₃ nanoparticles on genotoxic responses in human peripheral blood lymphocytes and cultured embryonic kidney cells. *J Toxicol Environ Health A* 76, 990-1002.

Di Bucchianico, S., Cappellini, F., Le Bihanic, F., Zhang, Y., Dreij, K., Karlsson, H.L., 2017. Genotoxicity of TiO₂ nanoparticles assessed by mini-gel comet assay and micronucleus scoring with flow cytometry. *Mutagenesis* 32, 127-137.

Di Virgilio, A.L., Reigosa, M., Arnal, P.M., Fernández Lorenzo de Mele, M., 2010. Comparative study of the cytotoxic and genotoxic effects of titanium oxide and aluminium oxide nanoparticles in Chinese hamster ovary (CHO-K1) cells. *Journal of Hazardous Materials* 177, 711-718.

Dušinská, M., Collins, A., 1996. Detection of Oxidised Purines and UV-induced Photoproducts in DNA of Single Cells, by Inclusion of Lesion-specific Enzymes in the Comet Assay. *Alternatives to Laboratory Animals* 24, 405-411.

ECHA, Registration dossier Aluminum oxide.

European Food Safety, A., 2008. Safety of aluminium from dietary intake - Scientific Opinion of the Panel on Food Additives, Flavourings, Processing Aids and Food Contact Materials (AFC). *EFSA Journal* 6, 754.

Ferraro, D., Anselmi-Tamburini, U., Tredici, I.G., Ricci, V., Sommi, P., 2016. Overestimation of nanoparticles-induced DNA damage determined by the comet assay. *Nanotoxicology* 10, 861-870.

Fontana, C., Kirsch, A., Seidel, C., Marpeaux, L., Darne, C., Gaté, L., Remy, A., Guichard, Y., 2017. In vitro cell transformation induced by synthetic amorphous silica nanoparticles. *Mutat Res* 823, 22-27.

Gao, C.-H., Mortimer, M., Zhang, M., Holden, P.A., Cai, P., Wu, S., Xin, Y., Wu, Y., Huang, Q., 2019. Impact of metal oxide nanoparticles on in vitro DNA amplification. *PeerJ* 7, e7228-e7228.

Hanas, J.S., Gunn, C.G., 1996. Inhibition of transcription factor IIIA-DNA interactions by xenobiotic metal ions. *Nucleic acids research* 24, 924-930.

Harris, W.R., Berthon, G., Day, J.P., Exley, C., Flaten, T.P., Forbes, W.F., Kiss, T., Orvig, C., Zatta, P.F., 1996. Speciation of aluminum in biological systems. *Journal of Toxicology and Environmental Health* 48, 543-568.

Hartmann, N.B., Jensen, K.A., Baun, A., Rasmussen, K., Rauscher, H., Tantra, R., Cupi, D., Gilliland, D., Pianella, F., Riego Sintes, J.M., 2015. Techniques and Protocols for Dispersing Nanoparticle Powders in Aqueous Media-Is there a Rationale for Harmonization? *J Toxicol Environ Health B Crit Rev* 18, 299-326.

Hashimoto, M., Imazato, S., 2015. Cytotoxic and genotoxic characterization of aluminum and silicon oxide nanoparticles in macrophages. *Dental Materials* 31, 556-564.

Heli, H., 2014. A study of double stranded DNA adsorption on aluminum surface by means of electrochemical impedance spectroscopy. *Colloids and Surfaces B: Biointerfaces* 116, 526-530.

Hussain, S.M., Hess, K.L., Gearhart, J.M., Geiss, K.T., Schlager, J.J., 2005. In vitro toxicity of nanoparticles in BRL 3A rat liver cells. *Toxicology in Vitro* 19, 975-983.

Ivask, A., , T., Tiina,, , V., Meeri, Vija, H., , K., Aleksandr,, Sihtmae, M., Pokhrel, S., Madler, L., Heinlaan, M., Kisand, V., Shimmo, R., Kahru, A., 2015. Toxicity of 11 Metal Oxide Nanoparticles to Three Mammalian Cell Types *In Vitro*. *Current Topics in Medicinal Chemistry* 15, 1914-1929.

Jalili, P., Gueniche, N., Lanceleur, R., Burel, A., Lavault, M.-T., Sieg, H., Böhmert, L., Meyer, T., Krause, B.-C., Lampen, A., Estrela-Lopis, I., Laux, P., Luch, A., Hogeveen, K., Fessard, V., 2018. Investigation of the in vitro genotoxicity of two rutile TiO₂ nanomaterials in human intestinal and hepatic cells and evaluation of their interference with toxicity assays. *NanoImpact* 11, 69-81.

Jalili, P., Huet, S., Lanceleur, R., Jarry, G., Le Hegarat, L., Nesslany, F., Hogeveen, K., Fessard, V., 2020. Genotoxicity of Aluminum and Aluminum Oxide Nanomaterials in Rats Following Oral Exposure. *Nanomaterials (Basel, Switzerland)* 10, 305.

Jenkinson, P., 2021. Critical Review of the Publications on the Genotoxicology of Aluminium Salts: 1990-2018. *Mutagenesis*.

Karlsson, H.L., Di Bucchianico, S., Collins, A.R., Dusinska, M., 2015. Can the comet assay be used reliably to detect nanoparticle-induced genotoxicity? *Environ Mol Mutagen* 56, 82-96.

Klotz, K., Weistenhöfer, W., Neff, F., Hartwig, A., van Thriel, C., Drexler, H., 2017. The Health Effects of Aluminum Exposure. *Dtsch Arztebl Int* 114, 653-659.

Krause, B., Meyer, T., Sieg, H., Kästner, C., Reichardt, P., Tentschert, J., Jungnickel, H., Estrela-Lopis, I., Burel, A., Chevance, S., Gauffre, F., Jalili, P., Meijer, J., Böhmert, L., Braeuning, A., Thünemann, A., Emmerling, F., Fessard, V., Laux, P., Lampen, A., Luch, A., 2018. Characterization of aluminum, aluminum oxide and titanium dioxide nanomaterials

using a combination of methods for particle surface and size analysis. *RSC Advances* 8, 14377 - 14388.

Krause, B.C., Kriegel, F.L., Rosenkranz, D., Dreijack, N., Tentschert, J., Jungnickel, H., Jalili, P., Fessard, V., Laux, P., Luch, A., 2020. Aluminum and aluminum oxide nanomaterials uptake after oral exposure - a comparative study. *Scientific reports* 10, 2698-2698.

Kumar, E., Bhatnagar, A., Kumar, U., Sillanpää, M., 2011. Defluoridation from aqueous solutions by nano-alumina: Characterization and sorption studies. *Journal of Hazardous Materials* 186, 1042-1049.

Lankoff, A., Banasik, A., Duma, A., Ochniak, E., Lisowska, H., Kuszewski, T., Gozdz, S., Wojcik, A., 2006. A comet assay study reveals that aluminium induces DNA damage and inhibits the repair of radiation-induced lesions in human peripheral blood lymphocytes. *Toxicol Lett* 161, 27-36.

Laux, P., Tentschert, J., Riebeling, C., Braeuning, A., Creutzenberg, O., Epp, A., Fessard, V., Haas, K.-H., Haase, A., Hund-Rinke, K., Jakubowski, N., Kearns, P., Lampen, A., Rauscher, H., Schoonjans, R., Störmer, A., Thielmann, A., Mühle, U., Luch, A., 2018. Nanomaterials: certain aspects of application, risk assessment and risk communication. *Arch Toxicol* 92, 121-141.

Le Hegarat, L., Dumont, J., Josse, R., Huet, S., Lanceleur, R., Mourot, A., Poul, J.M., Guguen-Guillouzo, C., Guillouzo, A., Fessard, V., 2010. Assessment of the genotoxic potential of indirect chemical mutagens in HepaRG cells by the comet and the cytokinesis-block micronucleus assays. *Mutagenesis* 25, 555-560.

Le Hégarat, L., Huet, S., Fessard, V., 2012. A co-culture system of human intestinal Caco-2 cells and lymphoblastoid TK6 cells for investigating the genotoxicity of oral compounds. *Mutagenesis* 27, 631-636.

Le Hégarat, L., Jacquin, A.G., Bazin, E., Fessard, V., 2006. Genotoxicity of the marine toxin okadaic acid, in human Caco-2 cells and in mice gut cells. *Environ Toxicol* 21, 55-64.

Le Hégarat, L., Mourot, A., Huet, S., Vasseur, L., Camus, S., Chesné, C., Fessard, V., 2014. Performance of comet and micronucleus assays in metabolic competent HepaRG cells to predict in vivo genotoxicity. *Toxicol Sci* 138, 300-309.

Li, X., Aldayel, A.M., Cui, Z., 2014. Aluminum hydroxide nanoparticles show a stronger vaccine adjuvant activity than traditional aluminum hydroxide microparticles. *Journal of controlled release : official journal of the Controlled Release Society* 173, 148-157.

Li, X., Zhang, C., Zhang, X., Wang, S., Meng, Q., Wu, S., Yang, H., Xia, Y., Chen, R., 2016. An acetyl-L-carnitine switch on mitochondrial dysfunction and rescue in the metabolomics study on aluminum oxide nanoparticles. *Part Fibre Toxicol* 13, 4-4.

Lima, P.D.L., Leite, D.S., Vasconcellos, M.C., Cavalcanti, B.C., Santos, R.A., Costa-Lotufo, L.V., Pessoa, C., Moraes, M.O., Burbano, R.R., 2007. Genotoxic effects of aluminum chloride in cultured human lymphocytes treated in different phases of cell cycle. *Food and Chemical Toxicology* 45, 1154-1159.

Magdolenova, Z., Collins, A., Kumar, A., Dhawan, A., Stone, V., Dusinska, M., 2014. Mechanisms of genotoxicity. A review of in vitro and in vivo studies with engineered nanoparticles. *Nanotoxicology* 8, 233-278.

Martin, K.R., Failla, M.L., Smith, J.C., 1997. DIFFERENTIAL SUSCEPTIBILITY OF CACO-2 AND HEPG2 HUMAN CELL LINES TO OXIDATIVE STRESS. *Journal of the Elisha Mitchell Scientific Society* 113, 149-162.

McKenna, D.J., Gallus, M., McKeown, S.R., Downes, C.S., McKelvey-Martin, V.J., 2003. Modification of the alkaline Comet assay to allow simultaneous evaluation of mitomycin C-induced DNA cross-link damage and repair of specific DNA sequences in RT4 cells. *DNA Repair* 2, 879-890.

Monteiro-Riviere, N.A., Oldenburg, S.J., Inman, A.O., 2010. Interactions of aluminum nanoparticles with human epidermal keratinocytes. *J Appl Toxicol* 30, 276-285.

Moradi, Z., Esmaili, M., Almasi, H., 2019. Development and characterization of kefiran - Al₂O₃ nanocomposite films: Morphological, physical and mechanical properties. *International Journal of Biological Macromolecules* 122, 603-609.

Narayan, R.J., Adiga, S.P., Pellin, M.J., Curtiss, L.A., Hryn, A.J., Stafslie, S., Chisholm, B., Shih, C.-C., Shih, C.-M., Lin, S.-J., Su, Y.-Y., Jin, C., Zhang, J., Monteiro-Riviere, N.A., Elam, J.W., 2010. Atomic layer deposition-based functionalization of materials for medical and environmental health applications. *Philos Trans A Math Phys Eng Sci* 368, 2033-2064.

OCDE, 2010. Test No. 487: In Vitro Mammalian Cell Micronucleus Test.

OECD, 2017. Guidance document on the in vitro Bhas 42 cell transformation assay. Series on Testing & Assessment No. 231.

Park, E.J., Sim, J., Kim, Y., Han, B.S., Yoon, C., Lee, S., Cho, M.H., Lee, B.S., Kim, J.H., 2015. A 13-week repeated-dose oral toxicity and bioaccumulation of aluminum oxide nanoparticles in mice. *Arch Toxicol* 89, 371-379.

Paz, L.N.F., Moura, L.M., Feio, D.C.A., Cardoso, M.d.S.G., Ximenes, W.L.O., Montenegro, R.C., Alves, A.P.N., Burbano, R.R., Lima, P.D.L., 2017. Evaluation of in vivo and in vitro toxicological and genotoxic potential of aluminum chloride. *Chemosphere* 175, 130-137.

Radziun, E., Dudkiewicz Wilczynska, J., Ksiazek, I., Nowak, K., Anuszezwska, E.L., Kunicki, A., Olszyna, A., Zabkowski, T., 2011. Assessment of the cytotoxicity of aluminium oxide nanoparticles on selected mammalian cells. *Toxicol In Vitro* 25, 1694-1700.

Rajiv, S., Jerobin, J., Saranya, V., Nainawat, M., Sharma, A., Makwana, P., Gayathri, C., Bharath, L., Singh, M., Kumar, M., Mukherjee, A., Chandrasekaran, N., 2016. Comparative cytotoxicity and genotoxicity of cobalt (II, III) oxide, iron (III) oxide, silicon dioxide, and aluminum oxide nanoparticles on human lymphocytes in vitro. *Hum Exp Toxicol* 35, 170-183.

Sabella, S., Carney, R.P., Brunetti, V., Malvindi, M.A., Al-Juffali, N., Vecchio, G., Janes, S.M., Bakr, O.M., Cingolani, R., Stellacci, F., Pompa, P.P., 2014. A general mechanism for intracellular toxicity of metal-containing nanoparticles. *Nanoscale* 6, 7052-7061.

Sadiq, R., Khan, Q.M., Mobeen, A., Hashmat, A.J., 2015. In vitro toxicological assessment of iron oxide, aluminium oxide and copper nanoparticles in prokaryotic and eukaryotic cell types. *Drug and Chemical Toxicology* 38, 152-161.

Saiyed, S.M., Yokel, R.A., 2005. Aluminium content of some foods and food products in the USA, with aluminium food additives. *Food Addit Contam* 22, 234-244.

Sakai, A., Sasaki, K., Muramatsu, D., Arai, S., Endou, N., Kuroda, S., Hayashi, K., Lim, Y.-m., Yamazaki, S., Umeda, M., Tanaka, N., 2010. A Bhas 42 cell transformation assay on 98 chemicals: The characteristics and performance for the prediction of chemical

carcinogenicity. *Mutation Research/Genetic Toxicology and Environmental Mutagenesis* 702, 100-122.

Sasaki, K., Mizusawa, H., Ishidate, M., 1988. Isolation and characterization of ras-transfected BALB/3T3 clone showing morphological transformation by 12-O-tetradecanoyl-phorbol-13-acetate. *Japanese journal of cancer research : Gann* 79, 921-930.

Shah, S.A., Yoon, G.H., Ahmad, A., Ullah, F., Amin, F.U., Kim, M.O., 2015. Nanoscale-alumina induces oxidative stress and accelerates amyloid beta (A β) production in ICR female mice. *Nanoscale* 7, 15225-15237.

Shepard, M.N., Brenner, S., 2013. An Occupational Exposure Assessment for Engineered Nanoparticles Used in Semiconductor Fabrication. *The Annals of Occupational Hygiene* 58, 251-265.

Shrivastava, R., Raza, S., Yadav, A., Kushwaha, P., Flora, S.J.S., 2014. Effects of sub-acute exposure to TiO₂, ZnO and Al₂O₃ nanoparticles on oxidative stress and histological changes in mouse liver and brain. *Drug and Chemical Toxicology* 37, 336-347.

Sieg, H., Braeuning, C., Kunz, B.M., Daher, H., Kästner, C., Krause, B.C., Meyer, T., Jalili, P., Hogeveen, K., Böhmert, L., Lichtenstein, D., Burel, A., Chevance, S., Jungnickel, H., Tentschert, J., Laux, P., Braeuning, A., Gauffre, F., Fessard, V., Meijer, J., Estrela-Lopis, I., Thünemann, A.F., Luch, A., Lampen, A., 2018. Uptake and molecular impact of aluminum-containing nanomaterials on human intestinal caco-2 cells. *Nanotoxicology* 12, 992-1013.

Sieg, H., Ellermann, A.L., Maria Kunz, B., Jalili, P., Burel, A., Hogeveen, K., Böhmert, L., Chevance, S., Braeuning, A., Gauffre, F., Fessard, V., Lampen, A., 2019. Aluminum in liver cells - the element species matters. *Nanotoxicology* 13, 909-922.

Sieg, H., Kästner, C., Krause, B., Meyer, T., Burel, A., Böhmert, L., Lichtenstein, D., Jungnickel, H., Tentschert, J., Laux, P., Braeuning, A., Estrela-Lopis, I., Gauffre, F., Fessard, V., Meijer, J., Luch, A., Thünemann, A.F., Lampen, A., 2017. Impact of an Artificial Digestion Procedure on Aluminum-Containing Nanomaterials. *Langmuir* 33, 10726-10735.

Simon-Deckers, A., Gouget, B., Mayne-L'Hermite, M., Herlin-Boime, N., Reynaud, C., Carrière, M., 2008. In vitro investigation of oxide nanoparticle and carbon nanotube toxicity and intracellular accumulation in A549 human pneumocytes. *Toxicology* 253, 137-146.

Sliwinska, A., Kwiatkowski, D., Czarny, P., Milczarek, J., Toma, M., Korycinska, A., Szemraj, J., Sliwinski, T., 2015. Genotoxicity and cytotoxicity of ZnO and Al₂O₃ nanoparticles. *Toxicology Mechanisms and Methods* 25, 176-183.

Som, C., Wick, P., Krug, H., Nowack, B., 2011. Environmental and health effects of nanomaterials in nanotextiles and façade coatings. *Environment International* 37, 1131-1142.

Song, Z.-M., Tang, H., Deng, X., Xiang, K., Cao, A., Liu, Y., Wang, H., 2017. Comparing Toxicity of Alumina and Zinc Oxide Nanoparticles on the Human Intestinal Epithelium In Vitro Model. *Journal of Nanoscience and Nanotechnology* 17, 2881-2891.

Tietz, T., Lenzner, A., Kolbaum, A.E., Zellmer, S., Riebeling, C., Gürtler, R., Jung, C., Kappenstein, O., Tentschert, J., Giubudagian, M., Merkel, S., Pirow, R., Lindtner, O., Tralau, T., Schäfer, B., Laux, P., Greiner, M., Lampen, A., Luch, A., Wittkowski, R., Hensel, A., 2019. Aggregated aluminium exposure: risk assessment for the general population. *Arch Toxicol* 93, 3503-3521.

Tsaousi, A., Jones, E., Case, C.P., 2010. The in vitro genotoxicity of orthopaedic ceramic (Al₂O₃) and metal (CoCr alloy) particles. *Mutat Res* 697, 1-9.

Turkez, H., Geyikoglu, F., Tatar, A., 2013. Borax counteracts genotoxicity of aluminum in rat liver. *Toxicol Ind Health* 29, 775-779.

Turkez, H., Yousef, M.I., Geyikoglu, F., 2010. Propolis prevents aluminium-induced genetic and hepatic damages in rat liver. *Food Chem Toxicol* 48, 2741-2746.

Verstraeten, S.V., Golub, M.S., Keen, C.L., Oteiza, P.I., 1997. Myelin Is a Preferential Target of Aluminum-Mediated Oxidative Damage. *Archives of Biochemistry and Biophysics* 344, 289-294.

Verstraeten, S.V., Oteiza, P.I., 2000. Effects of Al³⁺ and Related Metals on Membrane Phase State and Hydration: Correlation with Lipid Oxidation. *Archives of Biochemistry and Biophysics* 375, 340-346.

Villarini, M., Gambelunghe, A., Giustarini, D., Ambrosini, M.V., Fatigoni, C., Rossi, R., Dominici, L., Levorato, S., Muzi, G., Piobbico, D., Mariucci, G., 2017. No evidence of DNA damage by co-exposure to extremely low frequency magnetic fields and aluminum on neuroblastoma cell lines. *Mutation Research* 823, 11-21.

Wagner, A.J., Bleckmann, C.A., Murdock, R.C., Schrand, A.M., Schlager, J.J., Hussain, S.M., 2007. Cellular Interaction of Different Forms of Aluminum Nanoparticles in Rat Alveolar Macrophages. *The Journal of Physical Chemistry B* 111, 7353-7359.

Willhite, C.C., Karyakina, N.A., Yokel, R.A., Yenugadhati, N., Wisniewski, T.M., Arnold, I.M., Momoli, F., Krewski, D., 2014. Systematic review of potential health risks posed by pharmaceutical, occupational and consumer exposures to metallic and nanoscale aluminum, aluminum oxides, aluminum hydroxide and its soluble salts. *Crit Rev Toxicol* 44 Suppl 4, 1-80.

Yousef, M.I., Mutar, T.F., Kamel, M.A.E., 2019. Hepato-renal toxicity of oral sub-chronic exposure to aluminum oxide and/or zinc oxide nanoparticles in rats. *Toxicol Rep* 6, 336-346.

Zhang, D., Quayle, M.J., Petersson, G., van Ommen, J.R., Folestad, S., 2017a. Atomic scale surface engineering of micro- to nano-sized pharmaceutical particles for drug delivery applications. *Nanoscale* 9, 11410-11417.

Zhang, F., Cao, Q., Cheng, J., Zhang, C., An, N., Bi, S., 2009. Electrochemical and Spectrometric Studies of Double-Strand Calf Thymus Gland DNA Denatured by Al(III) at Neutral pH. *Analytical Sciences* 25, 1019-1023.

Zhang, Q., Wang, H., Ge, C., Duncan, J., He, K., Adeosun, S.O., Xi, H., Peng, H., Niu, Q., 2017b. Alumina at 50 and 13 nm nanoparticle sizes have potential genotoxicity. *J Appl Toxicol* 37, 1053-1064.

Zhang, R.-Y., Liu, Y., Pang, D.-W., Cai, R.-X., Qi, Y.-P., 2002. Spectroscopic and Voltammetric Study on the Binding of Aluminium(III) to DNA. *Analytical Sciences* 18, 761-766.

Zhao, J., Castranova, V., 2011. Toxicology of nanomaterials used in nanomedicine. *J Toxicol Environ Health B Crit Rev* 14, 593-632.

Table 1: Summary of NM characteristics as reported by the supplier.

NM	NM-code	Average particle size ^a (nm)	SSA ^b (m ² /g)	Purity ^c	Bulk density ^d True density ^d (g/cm ³)	Morphology
Al ⁰	NM-0015-HP	18	40-60	> 99%	2.70 0.008-0.20	spherical

Al ₂ O ₃	NM-0036-HP	20	<200	99%	- 0.9	spherical
ZnO	NM-0011-HP	20	50	99.5%	5.6 0.3-0.45	Nearly spherical

^a Average particle size was determined by TEM

^b Average specific surface area (SSA) was determined by Brunauer-Emmet-Teller (BET)

^c Purity was determined by X-ray Powder Diffraction (XRD)

^d Density was assessed by normal volumetric test

Table 2: Physico-chemical characterization of Al⁰, Al₂O₃ and ZnO NMs.

Sample (100 µg/ml)	Dispersion solution (0h)		Dispersion solution (24 h)	
	PdI	Z-Ave (d.nm)	PdI	Z-Ave (d.nm)
Al ⁰	0.173 ± 0.004	254 ± 4	0.159 ± 0.026	253 ± 12
Al ₂ O ₃	0.235 ± 0.015	168 ± 3	0.186 ± 0.021	160 ± 2
ZnO	0.104 ± 0.038	233 ± 11	0.112 ± 0.045	189 ± 18
	DMEM 10% FBS (0h)		DMEM 10% FBS (24h)	
Al ⁰	0.176 ± 0.011	197 ± 2	0.156 ± 0.011	201 ± 1
Al ₂ O ₃	0.521 ± 0.027	81 ± 1	0.337 ± 0.041	108 ± 1
ZnO	0.262 ± 0.010	198 ± 4	0.178 ± 0.019	156 ± 9
	William's 5% FBS (0h)		William's 5% FBS (24h)	
Al ⁰	0.158 ± 0.008	240 ± 14	0.152 ± 0.007	246 ± 12
Al ₂ O ₃	0.466 ± 0.015	107 ± 2	0.442 ± 0.018	120 ± 2
ZnO	0.233 ± 0.030	208 ± 6	0.165 ± 0.011	182 ± 11

The mean hydrodynamic diameter (Z-Ave) and polydispersity index (PdI) were determined in the stock dispersion solution and cell media (DMEM + 10 % FBS and William's + 5 % FBS) after 0 h and 24

h at a concentration of 100 $\mu\text{g}/\text{mL}$. Three independent experiments were performed. Results are expressed as mean \pm SD.

Table 3: Ion release from Al^0 , Al_2O_3 , ZnO NMs and AlCl_3 .

NMs	NM concentration ($\mu\text{g}/\text{mL}$)	Dispersion stock solution [%]	DMEM + 10%	William's +
			FBS [%]	5% FBS [%]
Al^0	25	1.30 ± 0.06	3.88 ± 0.13	2.42 ± 0.07
	50	0.85 ± 0.05	1.94 ± 0.09	1.26 ± 0.07
	100	0.48 ± 0.02	0.95 ± 0.04	0.68 ± 0.01
Al_2O_3	25	0.24 ± 0.04	0.40 ± 0.03	0.32 ± 0.11
	50	0.18 ± 0.03	0.48 ± 0.06	0.35 ± 0.07
	100	0.15 ± 0.01	0.37 ± 0.02	0.27 ± 0.02
AlCl_3	25	89.60 ± 5.97	57.16 ± 5.97	23.35 ± 0.26
	50	61.72 ± 0.77	30.09 ± 0.44	12.86 ± 0.28
	100	94.31 ± 6.61	17.54 ± 0.72	6.47 ± 0.52
ZnO	25	29.21 ± 0.53	85.09 ± 5.30	54.99 ± 1.03
	50	15.07 ± 0.10	57.97 ± 0.68	28.54 ± 1.18
	100	7.40 ± 0.05	30.21 ± 0.23	14.74 ± 0.21

Ion release was determined by ICP-MS in the stock dispersion solution and the cell media (DMEM + 10 % FBS and William's + 5 % FBS) after 24 h at concentrations of 25, 50 or 100 $\mu\text{g}/\text{mL}$. Data are presented as the mean \pm SD of three independent experiments.

Table 4: Detection of chromosomal damage in differentiated Caco-2 and HepaRG cells treated with Al-containing NMs. Cells were treated with increasing concentrations of Al^0 , Al_2O_3 and ZnO NMs, and with the ionic salt control AlCl_3 . MMS was used as a positive control (25 $\mu\text{g}/\text{mL}$ for Caco-2 cells and 30 $\mu\text{g}/\text{mL}$ for HepaRG cells). Results are presented as means (\pm SEM) of the percentage of binucleated micronucleated cells (BNMN) scored from 1000 binucleated cells per slide. Two slides per concentration were scored per experiment.

Viability was calculated by the replicative index (RI). Each concentration was tested in duplicate, $n=3$. The percentages of BNMN cells were compared using the one-way Pearson chi-square test.*** $p<0.01$.

		Caco2		HepaRG	
		%BNMN	RI (%)	% BNMN	RI (%)
Control	0	5.6 ± 0.3	100 ± 0	3.6 ± 0.5	100 ± 0
Al ⁰ NMs [µg/cm ²]	3	5.7 ± 0.4	97 ± 0.8	3.2 ± 0.3	97 ± 5.7
	9	5.7 ± 0.5	99 ± 3	3.2 ± 0.2	99 ± 3.1
	28	5.5 ± 0.4	103 ± 3.3	2.4 ± 0.2	101 ± 6.7
	40	5.9 ± 0.6	98 ± 2.6	3.5 ± 0.9	101 ± 5.5
	80	6 ± 0.5	94 ± 0.6	2.2 ± 0.3	110 ± 4.5
Al ₂ O ₃ NMs [µg/cm ²]	3	6.4 ± 1	102 ± 4	3.6 ± 0.6	99 ± 3.3
	9	5.6 ± 1.4	100 ± 2.9	3.3 ± 0.3	102 ± 5.2
	28	6.3 ± 1.4	96 ± 2.2	4.5 ± 0.8	109 ± 7.2
	40	6.4 ± 0.7	98 ± 0.7	3.5 ± 0.5	106 ± 6.8
	80	6.4 ± 1	102 ± 4	3.6 ± 0.6	99 ± 3.3
AlCl ₃ [µg/ml]	28	6.9 ± 0.5	103 ± 1.5	4.7 ± 1.5	114 ± 3.8
	40	6.9 ± 0.8	100 ± 1	4.3 ± 0.8	113 ± 3.3
ZnO NMs [µg/cm ²]	3	7 ± 0.8	100 ± 4.1	3.7 ± 0.4	96 ± 3.5
	6	8 ± 0.7	96 ± 3.8	4.1 ± 0.4	90 ± 3.4
MMS [µg/mL]		12.4 ± 0.6 **	39 ± 5.7 **	11.2 ± 2.4 **	96 ± 4.9

Table 5: Effects of Al-containing NMs on cell growth and foci numbers in the CTA assay in Bhas-42 cells. Cells were treated from day 1 to 4 (initiation assay) or from day 4 to 14 (promotion assay) with Al⁰ and Al₂O₃ NMs, and with AlCl₃ and post-cultivated in fresh medium until Day 21. MCA (1 µg/mL) and TPA (0.05 µg/mL) were included as positive controls. The mean of the cell growth (CG) and the number of transformed foci per well (foci/well) were measured from 3 and 6 replicate cultures respectively, according to the OECD.

Chemical	Concentration	Initiation assay		Promotion assay	
		CG ^a	Foci/well ^b	CG ^a	Foci/well ^b
Al	0 ^c (0.005% BSA)	100	5.3 ± 1.5	100	8.7 ± 3.1
	0.03 µg/cm ²	107	6.5 ± 1.4	99	4.7 ± 2.1 *

	0.1 $\mu\text{g}/\text{cm}^2$	105	5.3 ± 2.4	97	$0.7 \pm 0.8^*$
	0.3 $\mu\text{g}/\text{cm}^2$	96	4.2 ± 0.8	89	$0.7 \pm 0.8^*$
	1 $\mu\text{g}/\text{cm}^2$	62	$2.7 \pm 1.6^*$	83	Toxic ^d
	3 $\mu\text{g}/\text{cm}^2$	14	$1.5 \pm 0.8^*$	75	Toxic ^d
Al ₂ O ₃	0 ^c (0.005% BSA)	100	5.3 ± 1.5	100	8.7 ± 3.1
	0.3 $\mu\text{g}/\text{cm}^2$	106	$3.0 \pm 2.0^*$	103	$5.7 \pm 2.0^*$
	1 $\mu\text{g}/\text{cm}^2$	94	$3.3 \pm 1.5^*$	95	7.0 ± 1.3
	3 $\mu\text{g}/\text{cm}^2$	97	3.8 ± 0.8	93	$5.8 \pm 1.6^*$
	9 $\mu\text{g}/\text{cm}^2$	74	3.5 ± 1.9	83	$4.0 \pm 1.5^*$
	28 $\mu\text{g}/\text{cm}^2$	72	$2.3 \pm 1.6^*$	84	$0.7 \pm 0.5^*$
AlCl ₃	0 ^c (2.5% H ₂ O)	100	4.7 ± 1.6	100	6.8 ± 1.7
	3 $\mu\text{g}/\text{ml}$	96	4.7 ± 1.0	96	Toxic ^d
	9 $\mu\text{g}/\text{ml}$	78	4.3 ± 2.4	88	Toxic ^d
	28 $\mu\text{g}/\text{ml}$	16	4.0 ± 1.3	80	Toxic ^d
MCA	0 ^c (0.1% DMSO)	100	5.8 ± 1.9		
	1 $\mu\text{g}/\text{ml}$	17	$14.7 \pm 2.9^\ddagger$		
TPA	0 ^c (0.1% DMSO)			100	8.8 ± 2.1
	0.05 $\mu\text{g}/\text{ml}$			112	$20.3 \pm 3.0^\ddagger$

^a % of cell growth compared to that of vehicle control.

^b Average number of transformed foci/well \pm SD.

^c Vehicle control: final vehicle concentration of the working culture media in parentheses.

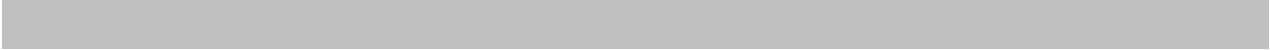
^d Absence of cells in well.

* $p < 0.05$; Dunnett test, vs vehicle control.

[‡] $p < 0.05$; *t*-test, vs DMSO (the vehicle of MCA and TPA).

Highlights

- Al⁰ and Al₂O₃ NMs did not induce chromosomal damage in the micronucleus assay.
- Al⁰ interference was observed in the comet assay.

- 
- Al₂O₃ induced DNA damage in the Fpg-modified comet assay although no significant ROS increase was observed.